INFLUENCE OF DISLOCATION MOBILITY ON THE YIELD IN SILICON-IRON

Thesis by

Donald Wayne Moon

In Partial Fulfillment of the Requirements

For the Degree of

Doctor of Philosophy

California Institute of Technology

Pasadena, California

1966

(Submitted May 27, 1966)

ACKNOWLEDGEMENTS

The author wishes to express his appreciation and indebtedness to: Professor Thad Vreeland, Jr. for his continued interest and everlasting patience during all phases of this research; Professor David S. Wood for his stimulating counsel and helpful suggestions; Mr. R. C. Blish and Mr. A. P. L. Turner for their assistance in experimentation and data reduction.

The experimental work was supported by financial assistance from the National Science Foundation and the Atomic Energy Commission.

ABSTRACT

This thesis presents the results of an experimental investigation of the yielding phenomenon during the transition from elastic to plastic behavior in 3 per cent silicon-iron alloy. Static load tests, constant strain-rate tests and square wave rapid loading tests were conducted on single crystal and polycrystalline specimens in order to determine the dislocation configurations at various stages in the yielding process. An electrolytic etching technique was used to reveal dislocation intersections with the observation surface.

Grain boundaries were found to be the primary source of dislocations for slip band formation in fully annealed material. The velocity of mobile dislocations was found to be an extremely sensitive function of the applied stress.

A true static upper yield point was found to be consistent with theories of the upper yield point based upon dislocation kinetics. The delay-time for yielding at constant applied stress was found to depend upon the dynamics of dislocation motion, the anisotropic stress concentration, the stress concentration due to relaxation of individual grains and the Schmid factor of the least favorably oriented grains.

Dislocation dynamics and dislocation configurations at various stages of plastic deformation were capable of accounting for a true upper yield point, the shape of the strain-time curve at constant stress and the Luder's band propagation velocity in polycrystalline specimens.

TABLE OF CONTENTS

TABLE OF CONTENTS--Continued

TABLE OF CONTENTS--Continued

LIST OF TABLES

LIST OF FIGURES

LIST OF FIGURES--Continued

I. INTRODUCTION

All materials deform when subjected to external loads. The deformation may be either elastic or plastic depending upon the magnitude of the applied stress and mechanical properties of the stressed material. Elastic deformation of crystalline materials is well understood and quite predictable because there is no rearrangement of interatomic bonds and no movement of lamellae of the crystal over one another. Mathematical standards for imitation or comparison (models) have been devised which describe elastic deformation quite adequately. On the other hand, plastic deformation does involve the rearrangement of interatomic bonds and the movement of lamellae over one another. The exact nature of plastic deformation is governed by mechanical phenomena occurring on the submicroscopic level. These phenomena have not been found to follow any a priori model. The complexities arising from interatomic bonding forces and motion of lamellae within a material are difficult to visualize and have thus far resisted representation by comprehensive mathematical models.

The most revealing approach to the problem of plastic deformation has been through the use of dislocation theory. The concept of a dislocation itself resulted from a careful interpretation of the observed fact that crystalline materials were not as strong as predicted from calculations based on interatomic bonding forces. The applicability of dislocation theory to the study of crystalline solids has been successfully established by direct observation of dislocations and their behavior. Dislocation concepts have been used to

explain the difference between the strengths of perfect crystals and imperfect crystals when the imperfections could be defined in terms of dislocation configurations. Some of the more obvious failures of dislocation theory have occurred when attempts were made to explain the behavior of materials subjected to large plastic strains. Many authors have proposed theoretical dislocation models which explain mechanical properties, plastic deformation and work hardening. These models are often contradictory and depend on critical assumptions which, with notable exceptions, can be verified by careful, though often tedious, experimental tests. These tests have not been performed. The purpose of this experimental investigation was to obtain dislocation data and observe dislocation motions and configurations in order to develop a more consistent and complete description of the transition from elastic to plastic deformation.

The progress of dislocation theory has to a large extent been limited by the lack of experimental evidence needed to verify the theory. One reason for the lack of experimental evidence has been the difficulty of observing dislocations. Several methods have been developed for revealing the presence of dislocations. Decoration by bulk diffusion of impurities has been used on some transparent materials and etching by chemical or electrolytic processes has been used on opaque materials to reveal dislocation intersections with free surfaces. In many cases a combination of decoration by bulk or surface diffusion followed by etching has been successfully used.

Diffraction contrast effects (1)* obtained by transmission electron microscopy reveal dislocations, and the dislocation motions can be observed directly. The use of the field ion microscope has made possible the direct observation of individual dislocation intersections with free surfaces. With the development of new tools for investigation and observation has come verification of some of the previous models and assumptions. In addition, the door has been opened for new experimentation and speculation on more complex problems with respect to the plastic deformation of materials. The common metals have been found to have similar mechanical properties when grouped according to the equilibrium crystalline lattice structures. It is reasonable to assume that the same model for plastic deformation would apply within a particular group having similar crystal structures.

Silicon-iron has been shown to exhibit many of the mechanical properties (e.g., pre-yield microstrain, upper yield point, discontinuous yielding and delay-time) commonly found in low-carbon steels and other body centered cubic (BCC) materials containing interstitial impurities (2, 3, 4, 5). The observation of dislocations is necessary in order to verify the dislocation models devised to describe these mechanical properties. Direct observation of dislocations is difficult due to their size. An etching technique for silicon-iron has

*Numbers appearing in parentheses indicate references listed at the end of the thesis.

been developed which reveals dislocation intersections with free surfaces (6). These intersections are revealed as pits on the surface after suitable decoration and etching.

The stress-strain curve shown in figure 1 is typical of fine grained silicon-iron. This curve is characteristic of static loading and is obtained when the strain rate is very low. The stress at the static upper yield point, σ_{uy}, decreases as the mean grain diameter is increased and disappears entirely at a critical grain size (7), only to reappear in single crystals. The grain size dependence of the stress at the static lower yield point, σ_{ly}, has been investigated by many people and is represented by the well-known Petch equation (8),

$$\sigma_{ly} = \sigma_f + k d^{-1/2} \qquad (1)$$

where σ_f is related to the friction stress on a moving dislocation within a grain, $k d^{-\frac{1}{2}}$ is the stress required to overcome the resistance to the spread of a slip band associated with a grain boundary and d is the mean grain diameter. The friction stress within a grain on a moving dislocation, τ_f, is the stress at which the first motion of unpinned dislocations is observed in the undeformed lattice, and is independent of grain size. Unpinned or "fresh" dislocations are those introduced into the material by scratching or other methods at temperatures low enough to prevent the migration of impurity atoms to the dislocation (9). Stresses greater than σ_f produce microstrain in grains containing the highest resolved

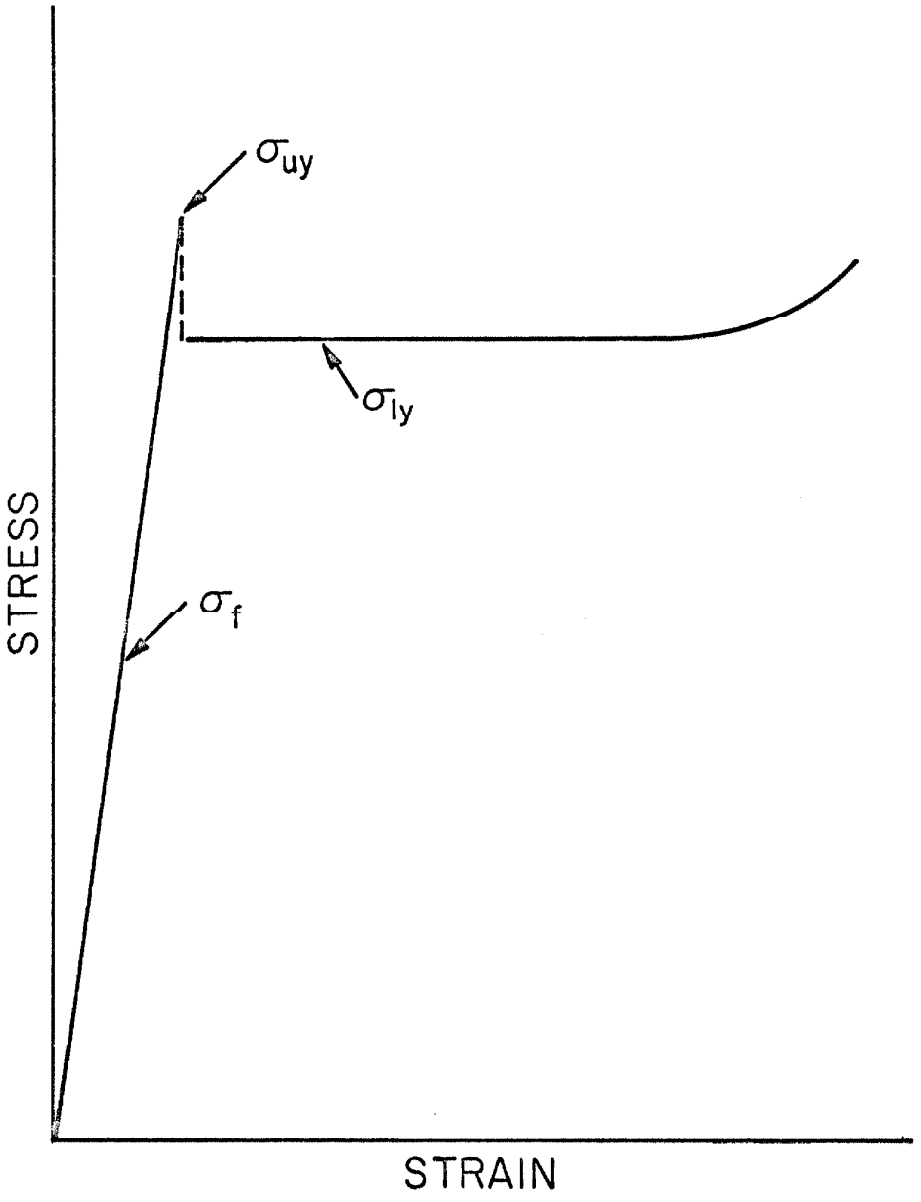

Fig. 1 Typical static stress-strain curve for fine grain silicon-iron.

shear stress (2). The stress required to produce plastic deformation in BCC materials containing interstitial impurities is sensitive to the rate of plastic deformation.

A familiar equation of basic dislocation theory for plastic shear strain, γ_p, is

$$\gamma_p = A b \tag{2}$$

where

A = total area of slip plane swept out by the dislocations per unit volume, and

b = magnitude of the Burgers vector associated with the dislocations.

The plastic shear strain-rate is given by

$$\dot{\gamma} = \dot{A} b \tag{3}$$

where

$$\dot{A} = \int_L v^* dl = \rho_m v, \tag{4}$$

v^* is the velocity of the moving dislocation segment dl, and L is the total length of dislocation line per unit volume. This integral cannot be evaluated directly, and has been simplified by the second equality in equation 4 where ρ_m is the total length of moving dislocation line per unit volume and v is the average velocity of moving dislocations. The total length of dislocation per unit volume of material ρ_T is proportional to the density of dislocation intersections on any reference plane through the material.

The constant of proportionality depends on the configuration of the dislocations on the slip planes and the orientation of the reference plane with respect to the slip planes. The constant of proportionality for silicon-iron is approximately unity and varies little for arbitrary reference planes (10). The units of ρ_T are length/volume, but the usual method of determining ρ_T is by the planar density, intersections/area. Throughout this thesis, the expression "dislocation density" will be used to denote the quantity ρ_T. Equation 3 has been used to express the relation between macroscopic shear strain-rate and microscopic dislocation parameters for both single crystal and polycrystalline specimens.

For a given material, the quantity b in equation 3 is entirely determined by the crystal lattice and operative slip system. The dynamic behavior of crystalline materials is therefore a direct function of the density of moving dislocations, ρ_m, and the velocity of moving dislocations, v. The mechanisms which create new dislocations will not be considered here. Large increases in dislocation densities always accompany the onset of plastic flow. These increases are often confined to narrow bands in the material and the densities within the bands approach a maximum due to dislocation interactions. However, Johnston and Gilman (11) infer that the flow of crystals is not limited by a lack of dislocations, but that dislocation mobilities must play an important part in determining the flow stresses of a crystal. It is significant to note that the above inference refers to flow of crystals and may exclude the

initiation of flow in view of locking by a mechanism such as the interaction of dislocations with interstitial impurities as proposed by Cottrell (12).

Certain plastic strain, which is small compared to elastic strain, occurs in materials subjected to stresses between σ_f and σ_{uy}. Since this strain occurs before the macroscopic yield point and is of very small magnitude, it has been called "pre-yield microstrain" to distinguish it from strain after attaining the upper yield point. Pre-yield microstrain has been experimentally investigated in silicon-iron under static loading conditions by Suits and Chalmers (2) and in low-carbon steel under rapidly applied constant stresses by Vreeland, Wood and Clark (3). The pre-yield microstrain observed in both of these investigations was found to approach a saturation value asymtotically for stress levels less than the upper yield stress and greater than the friction stress. The average equilibrium microstrain prior to the upper yield point was found to be 30×10^{-6} in./in. for low-carbon steel. A lower limit for ρ_m corresponding to the pre-yield microstrain can be estimated as follows. Suits and Chalmers have shown by etch pit studies that pre-yield microstrain is confined to individual grains. The average maximum distance a single dislocation can move is therefore the mean grain diameter of the material $\bar{d}$.

The total area of slip plane swept out by the moving dislocations is

$$A = \rho_m \bar{x} \qquad (5)$$

where $\bar{\chi}$ is the average distance the dislocations move. The smallest value of ρ_m occurs when $\bar{\chi}$ is a maximum for a fixed value for A. The maximum distance the dislocations can move during pre-yield microstrain is $\bar{d}$. Equation 2 can now be rearranged and the expression $A = \rho_m \bar{d}$ used to obtain a lower limit for ρ_m:

$$\rho_m = \gamma_p / b\bar{d} \qquad (6)$$

where γ_p is taken as one half the elongation strain. The lower limit for the total number of dislocations which must have moved is $\rho_m = 10^{+6}$ dislocations/in.^{2} using the values for b, $\bar{d}$ and ϵ_p obtained by Vreeland, Wood and Clark.

When the strain is increased beyond its value at the upper yield point, the load on the specimen decreases. This yield point drop is the most prominent feature of the plastic deformation characteristics for BCC materials with interstitial impurities. Clark and Wood (13) found that a well defined period of time elapsed between the instant the stress reached its full value and the instant plastic deformation began. This period of time is called the "delay-time." The limited strain sensitivity of the method of Clark and Wood made an observation of pre-yield microstrain impossible. However, these experiments established the existence of delay-time for macroscopic plastic strain in fully annealed low-carbon steel. The yield point drop was shown to be a time dependent phenomenon. A typical strain-time curve under constant applied stress for fine grain low-carbon steel is shown in figure 2. The strain sensitivity of the test is

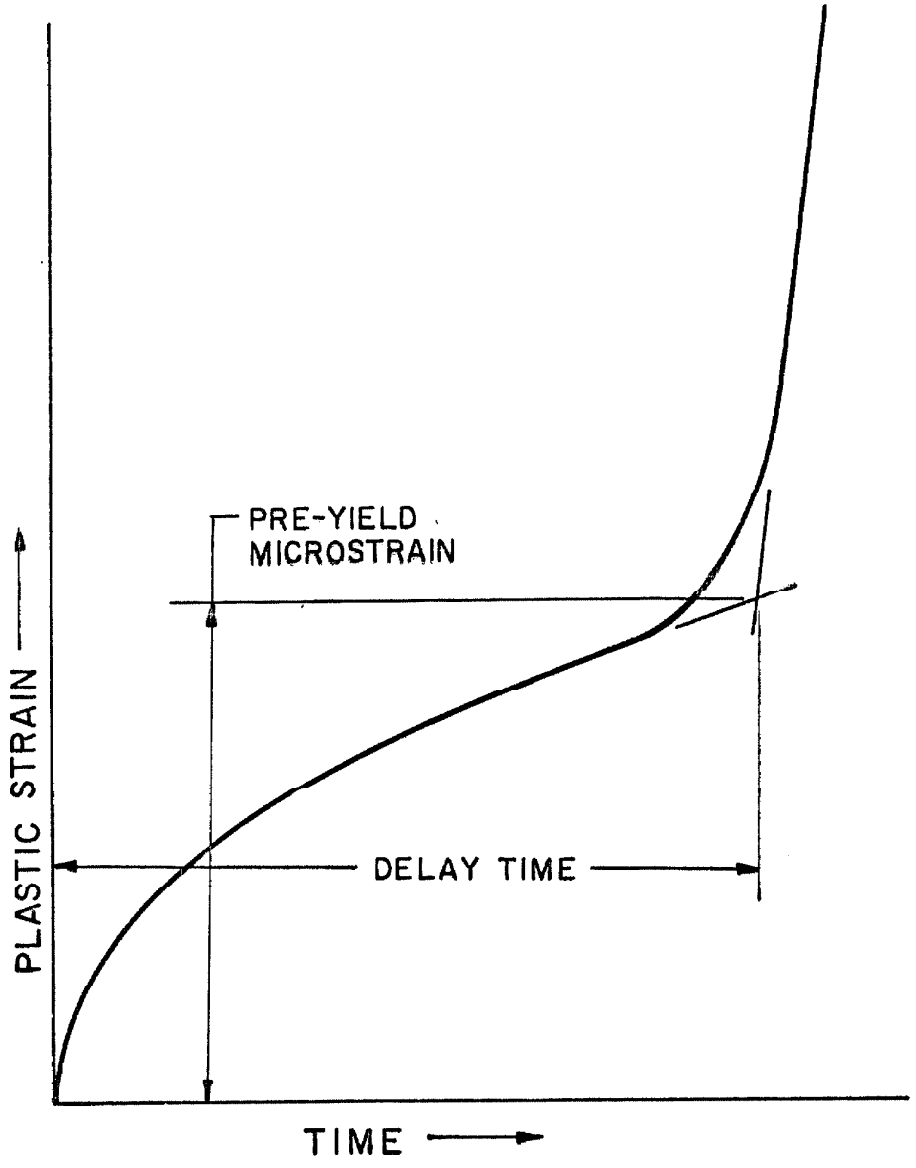

Fig. 2 Typical plastic strain-time curve for fine grain low-carbon steel under constant applied stress.

sufficient to demonstrate clearly pre-yield microstrain and the delay-time for yielding at constant applied stress.

Several theories for the existence of the upper yield point and associated phenomena have been based on the works of Cottrell. In his first theory (14) Cottrell attributed the sharp yield drop to the tearing away of dislocations from atmospheres of segregated carbon and nitrogen impurities. The decrease in stress at the beginning of plastic deformation was attributed to the reduced stress required to keep a dislocation in motion after it had been released from the atmosphere. After the observation of microstrain at stresses below the upper yield point, Cottrell modified his theory. The delay-time in Cottrell's modified theory (15) was the time required to form a pile-up of dislocations against an obstacle. This delay-time was due to the limited rate at which dislocations could be released from atmospheres under the combined action of stress and thermal fluctuations. The yield point drop thus emerged as the sudden breakdown of the obstacle blocking the pile-up. The breakdown occurred when the stress due to the pile-up was sufficient to overcome the obstacle and propagate dislocations beyond the barrier. Cottrell's modified theory and later models (12) based on the modified theory thus contained the essential features of the experimentally observed yield point drop, delay-time and pre-yield microstrain.

Fisher (16) applied Cottrell's theory (15) to the delayed yield in mild steel and obtained good agreement with experimental observations for the temperature and stress dependence. However, he found

that unreasonably low values of binding energy between interstitial atoms and dislocation lines were required in order to fit Cottrell's theory to observed delay-time. Cottrell (17) modified Fisher's treatment of thermally activated release of dislocations and obtained reasonable values of the parameters in the theory when applied to delay-time measurements.

Russell, Wood and Clark (18) modified Cottrell's treatment and thereby explained the grain size effect on delay-time by assuming that a critical fraction of the total number of grains must contain piled-up groups of dislocations before the onset of macroscopic yielding. They assumed that a Luder's band is formed by the growth of yielded regions. The growth is unstable because of the stress concentration at the interface between the yielded and unyielded regions of the materials. They obtained reasonable agreement with the experimental measurements. All of the above theories of the yield drop and delay-time treated the rate determining process in yielding as the thermally activated release of dislocations from Cottrell atmospheres. An alternative hypothesis is that the delay-time may be governed by the velocity with which dislocations move once they have been created or released from a pinned position. This alternative has resulted from direct observations of slip band structures and dislocation velocities.

Direct observations of the structure of slip bands in silicon-iron by etch pit techniques (19) and by electron microscopy (20) suggest that the bands are not formed by the dynamic generation of a

large number of loops from a single source. The double cross-slip mechanism proposed by Koehler (21) appears to operate after the initial source has generated at most a small number of loops, and this mechanism accounts for the multiplication and spread of the slip band. The slip band growth is fastest in the direction of the Burgers vector since the leading edge segments of the slip band do not cross-slip and interact with loops growing on nearby slip planes.

Direct observation of the average velocity of mobile dislocations has been made in lithium-fluoride (11) and silicon-iron (9). Johnston and Gilman (11) have shown that for velocities well below the shear wave speed in LiF the velocity is a very sensitive function of the applied stress and that there is a minimum stress below which no dislocations move. The velocity of glide dislocations has as an upper limit the shear wave speed or "velocity of sound" in the crystal. This results from the increase in kinetic energy associated with the dislocation as it moves through the crystal (22). Stein and Low (9) have shown that for 3 1/4 per cent silicon-iron the average velocity of moving dislocations, v, is an extremely sensitive function of the applied stress. For a constant temperature, the data of Johnston and Gilman have been fitted to the empirical relation $v = v_c e^{-D/\tau}$ where v_c is the shear wave speed in the material, D is a material constant and τ is the applied stress. Their data have also been fitted to the empirical relation (23)

$$v = \left(\tau/\tau_o\right)^n \qquad (7)$$

for velocities well below v_c , where τ_o is the stress necessary for a velocity of 1 cm/sec. Stein and Low have fitted their data for silicon-iron to equation 7.

The next development in the theory of the yield point took place with the application of the strain rate equation 3. Johnston (23) has accurately predicted the stress-strain curve for single crystal specimens of LiF. He started with equation 7, assumed a linear relation between ρ_m and γ of the form $\rho_m = \rho_o + \alpha\gamma$ and accounted for the elastic strain in the loading device. Johnston had experimentally determined the values of α , n and τ_o for his material. The two parameters found to be most critical in his work were the values of ρ_o and the exponent n in equation 7. The stiffness of the testing machine and exact nature of the dislocation multiplication process were of secondary importance in obtaining a yield drop. The delay-time for yielding in LiF single crystals as interpreted by Johnston was attributed to the incubation period necessary to generate a measurable value of the product $b\rho_m v$ at the constant applied stress. Thus the dynamics theory of Johnston was shown to predict accurately both the static and dynamic plastic deformation for LiF single crystals.

Hahn (4) and later Cottrell (24) have applied Johnston's dynamic theory to polycrystalline specimens. As with the Fisher treatment, for different reasons, Hahn obtains the correct stress and temperature dependence for the delay-time. The yield point drop in polycrystalline iron is found to depend quite critically on the

value of n in equation 7 and the initial density of mobile dislocations ρ_o . Hahn's treatment does not explain the disappearance of the yield drop with increasing grain size (18), does not consider pre-yield microstrain or mobile dislocations produced by pre-yield microstrain and does not consider the heterogeneous nature of the polycrystalline material in the yielding mechanics. In a recent publication, Petch (25) has presented an empirical equation for the upper yield point which, like his lower yield point equation, depends on $d^{-1/2}$ but does not consider the effect of the polycrystalline nature of the material on the microdynamics of dislocations or on the dislocation configurations which develop.

All of the above theories and models for the plastic deformation of polycrystalline materials suffer from a lack of good experimental observations on the microscopic scale. This lack of experimental evidence forces assumptions to be made at critical stages in the development of the models and theories. Several assumptions are common to most of the above theories. Some of the areas in which careful experimental work would lead to a better understanding of the dislocation processes related to yielding are discussed below.

Uncertainties in material constants and exact dislocation configurations force the assumption of homogeneity and the use of average values for parameters which are known to be heterogeneous and dependent upon time, strain, temperature, etc.

The sources of mobile dislocation in both single and polycrystalline specimens have been assumed by most authors to be

uniformly distributed throughout the bulk of the materials initially, and the probability of each one becoming active has been assumed to be initially the same. The assumption that the sources and probabilities remain uniformly distributed and equal during the transition from microstrain to fully developed uniform yielding is not always reasonable. The operation of a single isolated source of dislocations will alter the probability distribution in the immediate vicinity of the active source by relaxation of the stress on the source by local plastic deformation. Similarly, the yielding of a single grain in a polycrystalline matrix will increase the average stress on the adjacent grains and thus alter the probability that these grains will begin to yield. Release times of dislocations from Cottrell atmospheres do not appear to be the rate determining process on the basis of the observed growth of slip lines and the proposed multiplication mechanisms of double cross-slip (19, 21).

Stress vs. dislocation velocity measurements have been directly made only for single crystal specimens of silicon-iron and tungsten (26) of the BCC metals. The exact stress distribution in a polycrystalline specimen is of course complicated because of elastic anisotropy. The extreme sensitivity of individual dislocation velocity to applied stress and the complicated stress distribution present a critical problem in predicting yielding behavior of polycrystals. A method of eliminating this problem would be to determine by direct observation the average velocity of individual dislocations in polycrystals.

The above theories predict strain-time curves at constant stress which are monotonically increasing functions of time in contrast to the observed inflection point behavior actually obtained for polycrystalline materials such as BCC iron. Hahn (4) has made essentially the same assumptions as Johnston, but has attempted to apply them to polycrystalline materials directly. Grain size and grain boundary effects have been totally ignored and hence the arguments presented are only applicable to single crystal specimens and are incapable of giving a truly static upper yield point.

The experimentally documented pre-yield microstrain (2, 3) does not eliminate the yield point drop or the delay-time for yielding in low-carbon steel and silicon-iron. Based on equation 2, this observed microstrain must certainly produce an abundance of mobile dislocations which contributes to subsequent deformation. Thus, the models presented in the literature apparently fail to describe plastic deformation in polycrystalline specimens for at least two reasons: a) they require that the initial dislocation density ρ_o be less than that produced during pre-yield microstrain; b) they predict strains which increase monotonically with time at constant applied stress levels greater than the static upper yield point.

There were two objectives of this experimental investigation. One was to obtain new data on the microdynamics of dislocations and the dislocation configurations during the transition from the upper yield stress to the lower yield stress. The second was to examine the current theories and models as they relate to the plastic

deformation of silicon-iron in order to obtain a better understanding of the macroscopic behavior of BCC materials with interstitial impurities.

An experimental program using the etch pit technique for direct observation of dislocation configurations was undertaken. Single crystal and polycrystalline specimens of iron-3.14 per cent silicon alloy were prepared as described in Part II. Constant strain rate and rapidly applied constant stress pulse tests were conducted in order to obtain dislocation mobility data as well as macroscopic stress-strain and strain-time data. The equipment used to obtain the data is described in Part III and the test procedures employed are given in Part IV.

The results of the testing program are presented in Part V. In addition to the experimental results, Part V contains comparisons with similar data reported previously and limitations of the data obtained here. A careful comparison of some of the critical assumptions in the above referenced literature with the new evidence presented here appears in Part VI. A more complete description of dislocation processes leading to the yielding of polycrystalline material is made possible by the observations of this investigation.

II. PREPARATION OF TEST SPECIMENS

Material

The material used in this investigation was obtained in strip form 2 inches wide and 0.024 inches thick. The General Electric Research Laboratory kindly supplied the following chemical analysis.

Element	Weight Per Cent
Silicon	3.14
Carbon	0.001
Manganese	0.043
Phosphorus	0.008
Sulphur	0.018
Nickel	0.066
Copper	0.079
Tin	0.010
Chromium	Trace
Aluminum	Trace
Iron	Remainder

This material is from the same heat as that used by Suits and Chalmers in their investigation (2).

Suits and Low (27) have reported that an iron silicon alloy must contain a carbon content from 0.004 to 0.006 wt. per cent in order for dislocation sites to be revealed by the Dunn and Daniels etching technique (6). The as-received strip stock was gas carburized to increase the carbon content to approximately 0.005 wt. per cent by the Angeles Heat Treating Company, Los Angeles, California. The carburizing atmosphere was derived from natural gas and contained water vapor as the controlling variable. The strip stock was carburized for 5 minutes in a batch type furnace maintained at 1550°F. The "Dew Point" of the carburizing atmosphere was 58-60°F.

Test Specimens

Drawings of the test specimens used in this investigation are shown in figures 3 and 4. Two thicknesses of polycrystalline specimens were used. The grain size and initial dislocation density are very sensitive to the amount of cold work prior to recrystallization. A "trial and error" procedure was used to determine a combination of cold working by rolling and heat treatment that would produce two different grain sizes with similar initial dislocation densities. Single crystal test specimens were fabricated by cementing loading tabs to the ends of the single crystals with Armstrong A-12 epoxy cement as shown in figure 4. This technique permitted the use of the same loading fixture for both polycrystals and single crystals.

Polycrystalline Specimens - Fine Grain

The carburized strip stock was rolled to obtain a 50 per cent reduction in area. Specimens of the shape shown in figure 3 were then formed with a blanking die. The blanked specimens, 0.010 in. thick, were recrystallized at 1290°F for one hour in a vacuum of not greater than one micron of mercury to prevent oxidation of the surface. The mean grain diameter after recrystallization was approximately 0.001 inches and the specimen contained an initial dislocation etch pit density of 10^6 to 10^7 per cm^2. The dislocation density could have been reduced by recrystallization at higher temperatures and longer times, but larger grains would have been produced.

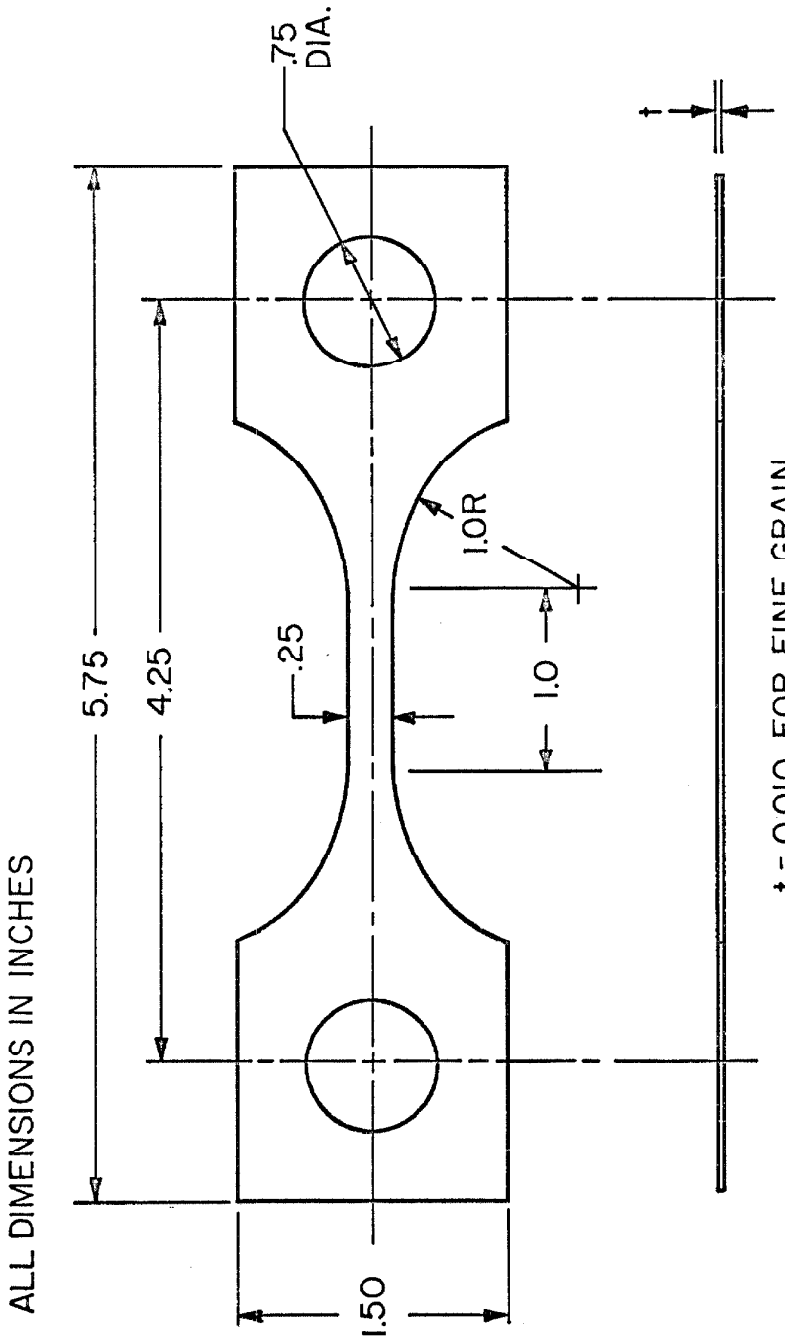

Fig. 3 Polycrystalline test specimen drawing.

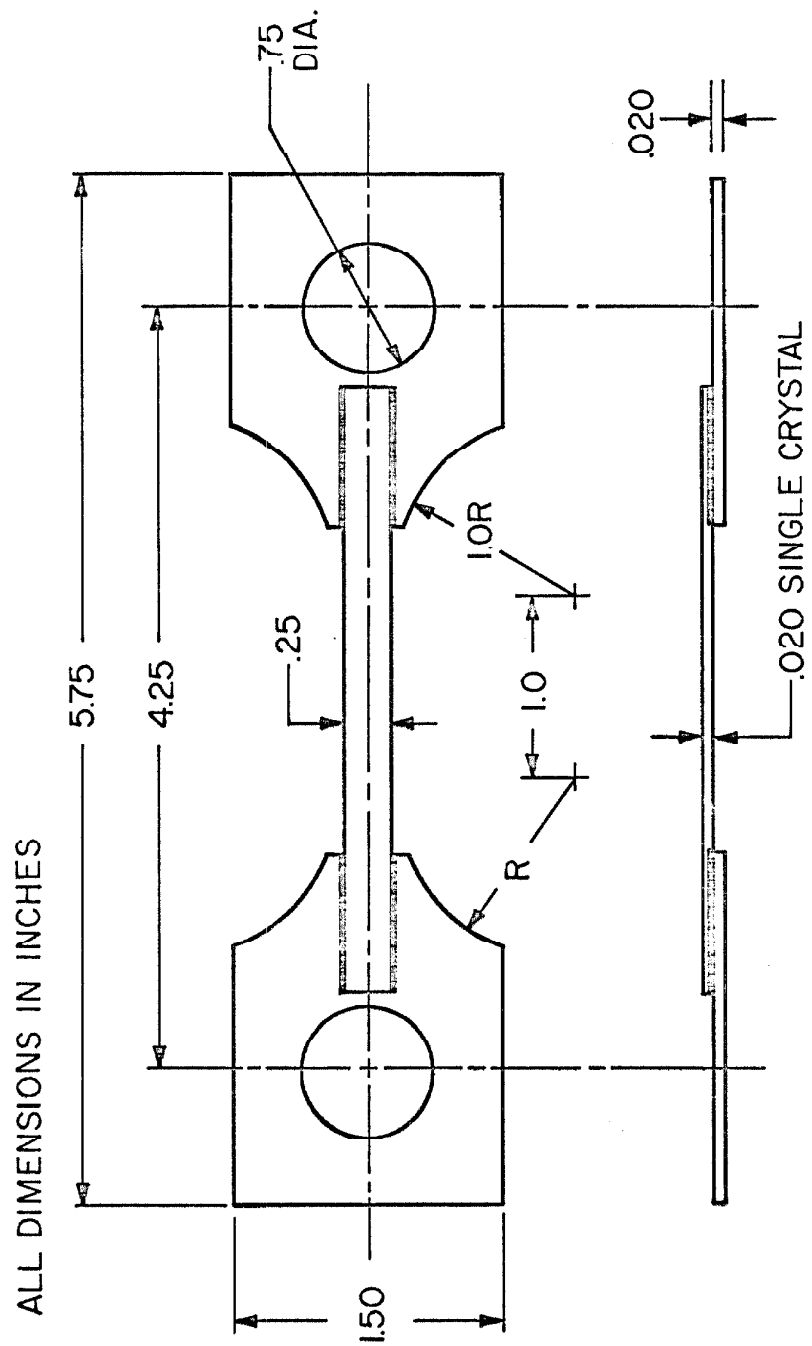

Fig. 4 Single crystal test specimen drawing.

In order to obtain a sharp upper yield point in a fine grained tensile specimen it is necessary to minimize bending stresses. This is particularly difficult in thin tensile specimens because of the difficulty in making the tensile axis pass through the centroid of the cross-section. The ratio of bending stress to tensile stress for a tensile specimen with rectangular cross-section is

$$\sigma_B / \sigma_T = 6e/t \qquad (8)$$

where

e = eccentricity of the load axis, and

t = specimen thickness.

Specimen curvature was found to cause an excessively large value of e after recrystallization of free hanging specimens.

The initial curvature was reduced by the use of a special fixture for holding the specimens during recrystallization. A drawing of this fixture is shown in figure 5. The fixture was made of 18-8 stainless steel, and one specimen was clamped to each side. Mica sheets were placed between the stainless steel and specimens to prevent fusion during the heat treatment. Stainless steel has a larger coefficient of thermal expansion than silicon-iron, which imposes tension on the two specimens as the temperature of the furnace is increased. This procedure straightens the specimens and insures their straightness during recrystallization. The fixture contracts more than the specimen as the temperature is decreased during cool-down, opening a gap at the butt face A of the fixture and thereby

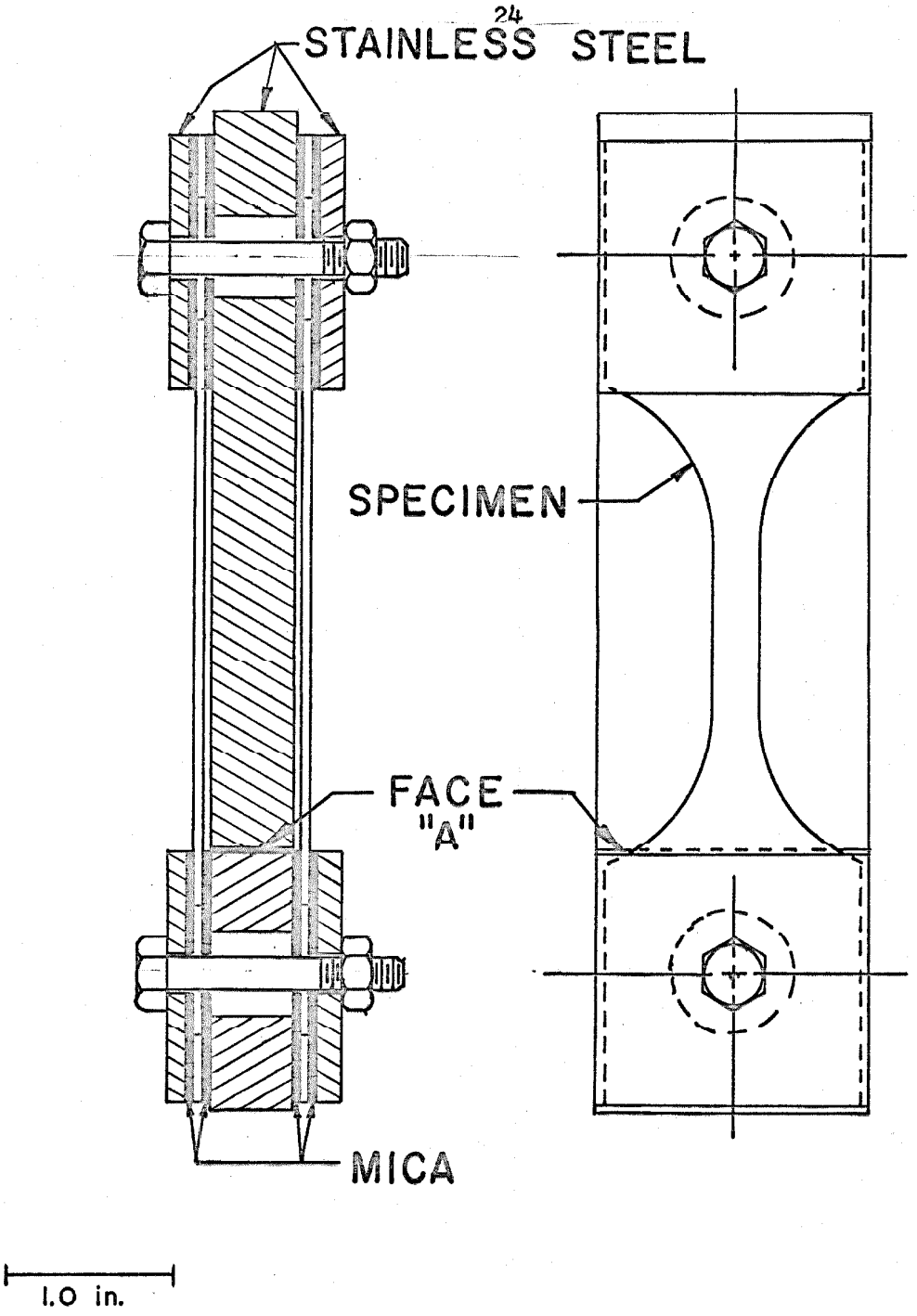

Fig. 5 Cross-section drawing of heat treatment fixture for recrystallization of blanked specimens.

preventing buckling of the specimens. This procedure reduced the bending stress due to initial specimen curvature to less than 1 per cent of the tensile yield stress.

Polycrystalline Specimens - Coarse Grain

The carburized strip stock was rolled to obtain a 6 per cent reduction of area. Specimens were then blanked to the shape shown in figure 3. The blanked specimens were recrystallized at 1850°F for one hour in vacuum as before. The coarse grained specimens were approximately 0.020 inches thick with a mean grain diameter of about 0.003 inches and initial dislocation density of 10^6 to 10^7 per cm^2.

Single Crystal Specimens

Single crystal specimens were produced by the strain-anneal method of Dunn and Nonken (28). The carburized strip stock was rolled to obtain a 6 per cent reduction of area. Strips approximately 4 inches long, 0.27 inches wide and 0.020 inches thick were sheared from stock. Several strips were stacked and clamped between 1/4 inch cold rolled steel bar stock with the sheared edges of the strips extending beyond the clamping bar. The exposed edges were ground flush with the bar on metallographic papers with final grinding on 600A silicon-carbide paper. This technique produced strips with less than 0.0005 in./in. of taper in width. Individual strips were suspended in the vacuum furnace and recrystallized at 1600°F for thirty minutes. The recrystallized strips were then "critically" strained in tension to approximately 3 per cent elongation which corresponded to the

Luder's strain for this material.

Various crosshead speeds were used during the critical straining of the annealed strips and load vs. time curves were recorded on the Instron X-Y chart recorder. This data will be discussed further in Part IV.

The remainder of the steps for producing single crystal strips may be summarized as follows (28):

1. One or more crystals were grown on one end of the strip by passing it slowly into the hot zone of a high temperature gradient furnace for about 1/2 inch.

2. The strip was removed from the furnace and etched with a 25 per cent solution of nitric acid to reveal the crystals which were produced in step 1. One of these crystals was chosen as the seed crystal and the remainder were removed by grinding.

3. All ground surfaces were heavily etched with a 25 per cent solution of nitric acid to remove possible nucleation sites from which new crystals could form.

4. The strip was returned to the furnace and passed into the hot zone through the high temperature gradient causing the seed crystal to grow through the entire strip.

A type 2904 vacuum furnace manufactured by NRC Equipment Corp., Newton Highlands, Massachusetts was used for all recrystallization and straightening heat treatment of specimens. The basic furnace consists of a heating unit enclosed within a stainless steel vacuum chamber. The heating unit is a water jacketed resistance furnace using tungsten heating elements with radiation shielding on the hot zone. The heating unit was modified to provide the high temperature

gradient ($\approx$ 1800°F per in.) required for single crystal growth. A cross-section of the heating unit with the modification is shown in figure 6. The temperature gradient achieved is shown in figure 7.

The single crystal specimens as produced by the above procedure would not etch properly to reveal dislocations. The portion of the single crystal immediately behind the growing front showed a "cell" type pattern. The cell boundaries were regions which did not show any dislocation etch figures. The interior of the cells revealed dislocation etch figures in the normal manner. At distances of a few thousandths of an inch behind the growing front, the cell began to fade out and had disappeared entirely at 1/8 in. behind the growth front. The cell type pattern very closely resembled the normal microstructure of the polycrystalline strip and the cell walls could readily be seen to align with grain boundaries across the growth front.

The probable explanation of this etching behavior is as follows. The carbon and impurity content in the grain boundaries of the polycrystalline strip was higher than that within the grains. The growth of the single crystal into the matrix was rapid enough to localize the carbon and impurities at the region of the former grain boundary. This region would not etch properly to reveal dislocation sites. At large distances from the single crystal growth front, the impurities and carbon had diffused throughout the crystal, thus changing the etching characteristics.

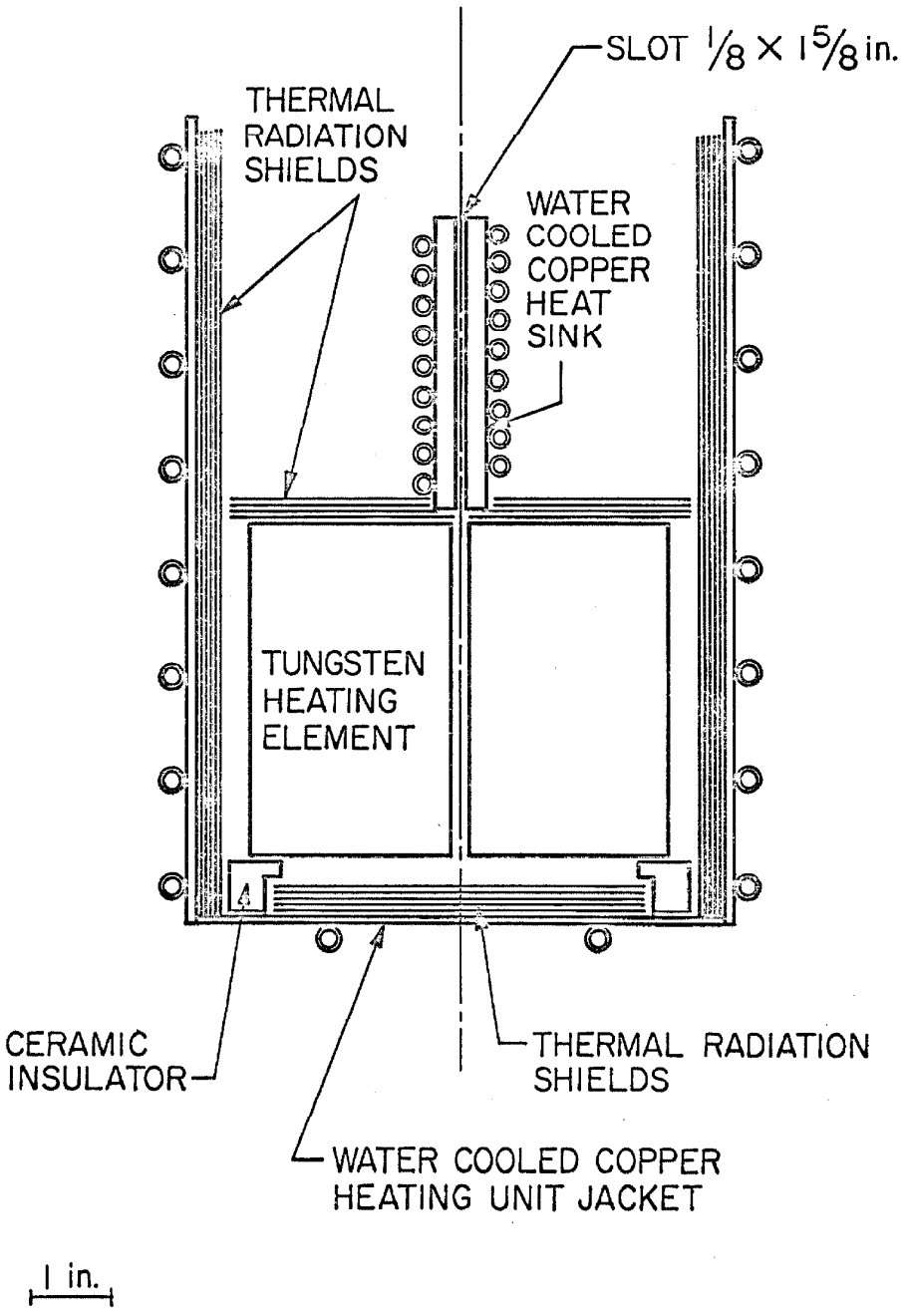

Fig. 6 Cross-section of vacuum furnace heating unit modified to provide a high temperature gradient.

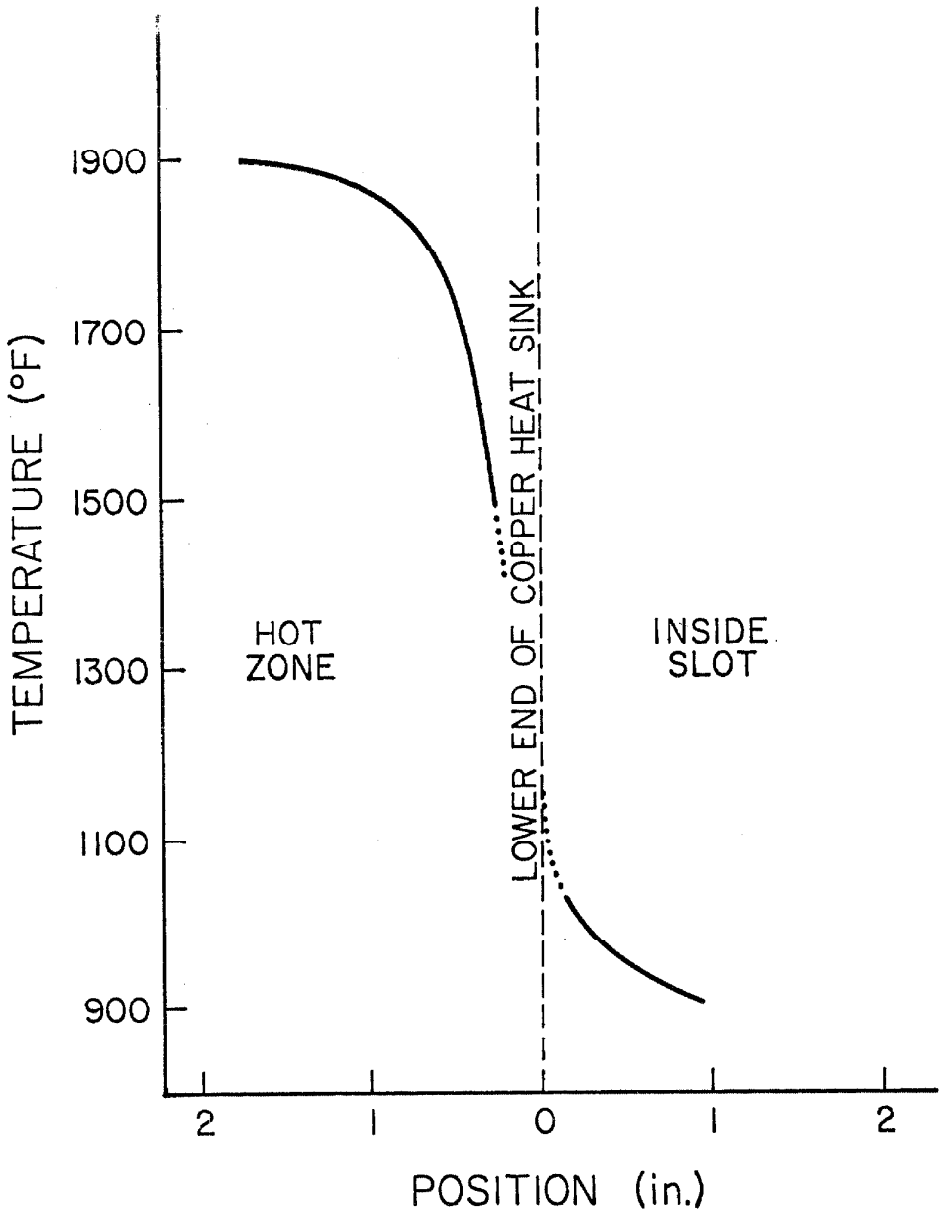

Fig. 7 Temperature variation with position in high temperature gradient furnace.

This unsatisfactory etching behavior of the single crystals was corrected. Carbon was removed from the single crystals by a 24 hour wet hydrogen treatment to reduce the carbon in solution to less than 0.001 per cent. The hydrogen was treated by passing it through the following equipment prior to entering the furnace which was maintained at 1290°F:

1. De-oxo catalytic hydrogen purifier, a product of Baker and Company, Newark, New Jersey.
2. Distilled water bath at 176°F with a 5 micron porous ceramic diffuser.
3. Heated manifold to prevent condensation.

The etch pitting of dislocation sites was made possible by increasing the carbon content to 0.005 per cent. A ten hour treatment in an atmosphere of dry hydrogen with one per cent methane by volume was used for the carbon addition (29). The hydrogen was passed through the following equipment before addition of the methane and introduction into the furnace which was maintained at 1560°F:

1. De-oxo catalytic hydrogen purifier.
2. Dri-rite ($CaSO_4$) drying tower.
3. Activated charcoal tower submerged in liquid nitrogen.

A slight curvature was introduced in the single crystals during the wet hydrogen and recarburization treatments. The single crystals were straightened by clamping them between flat strips of hot rolled steel and heating the assembly to 1560°F for two hours in vacuum. The straightened single crystals were used to fabricate tensile specimens.

An alignment fixture was used to hold the single crystal strip accurately positioned on the center-line established by the two holes in the loading tabs during the curing cycle for the epoxy cement. Figure 8 is a photograph of the alignment fixture with a specimen in place ready for the curing cycle.

This alignment fixture was capable of maintaining less than 0.001 inches of misalignment between the center-line of the loading tab holes and the center-line of the single crystal strip. The essential feature of this fixture was that it would accept all widths of single crystal strips between 0 and 3/8 inches and still maintain the above accuracy of alignment without recourse to measuring instruments, while requiring a minimum amount of set-up time.

The orientation of each single crystal was determined by the back-reflection Laue method after fabrication of the specimen. The location of the tensile axis for each crystal is shown in the unit stereographic triangle, figure 9.

A summary of the specimens prepared for this investigation, their grain size and the nominal dislocation etch pit density is given below.

Specimen	Grain Size, in.	Etch Pit Density, cm^{-2}
Fine Grain Polycrystal	0.001	10^6 - 10^7
Coarse Grain Polycrystal	0.003	10^6 - 10^7
Single Crystal	0.020 x 0.25 x 3	10^6 - 10^7

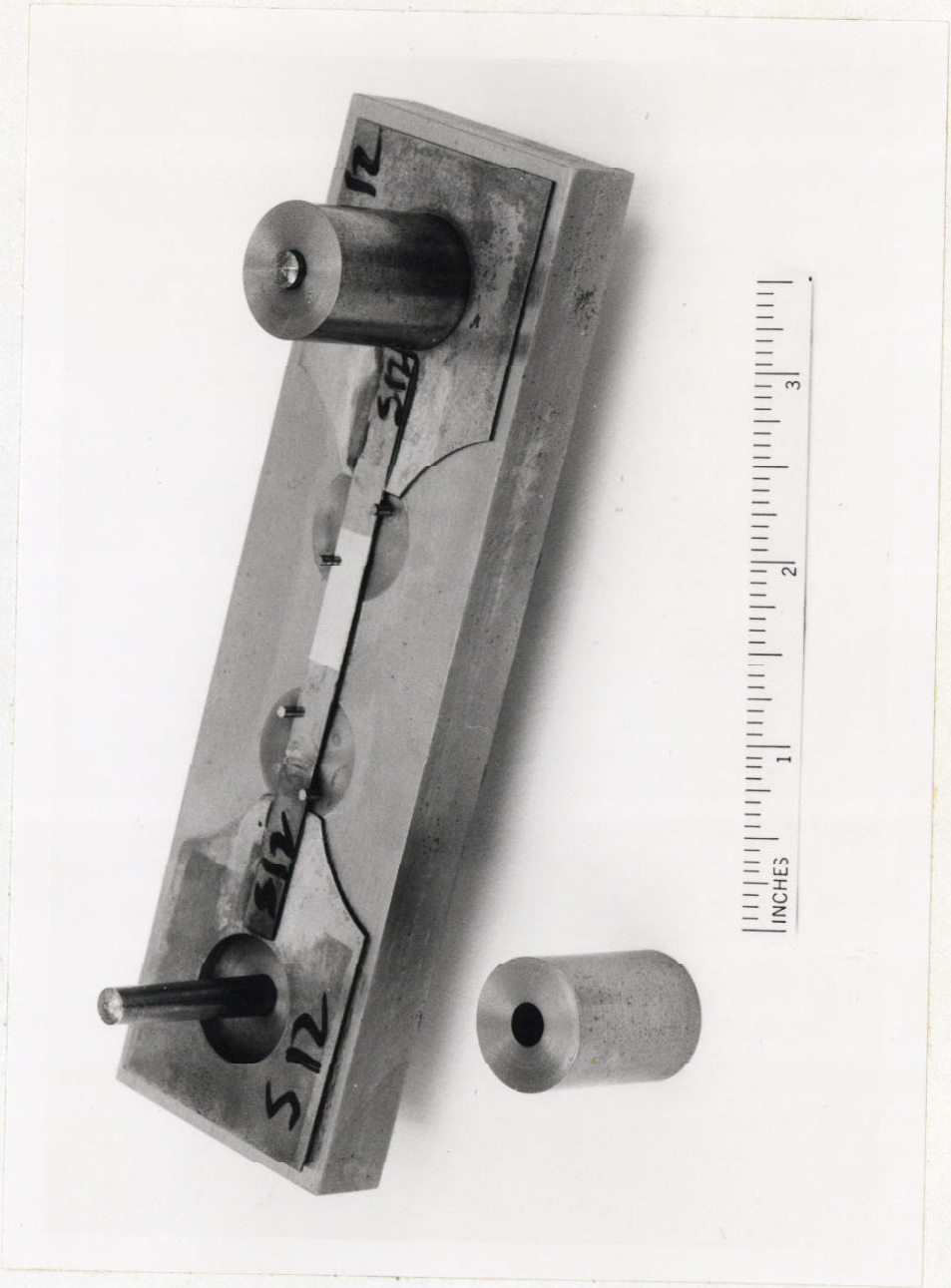

Fig. 8 Single crystal alignment fixture used during fabrication of test specimens.

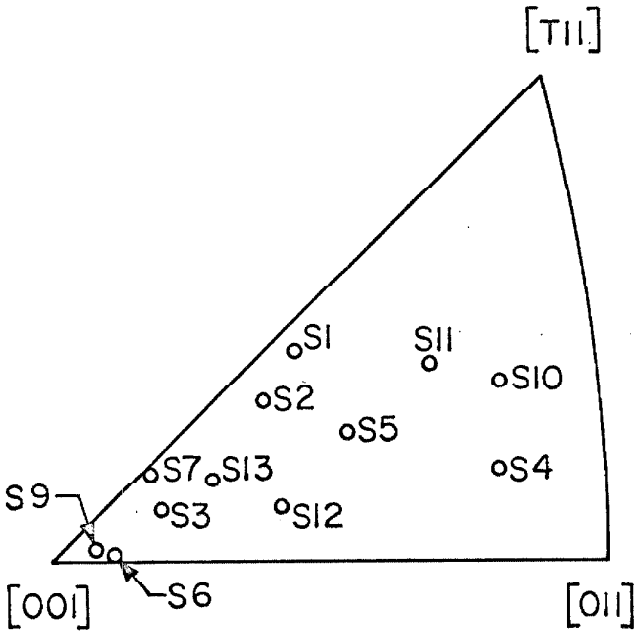

Fig. 9 Unit stereographic triangle showing location of tensile axis for all single crystal specimens.

III. TEST EQUIPMENT AND TECHNIQUES

Rapid Load Testing Machine

The equipment for rapid load testing shown in figure 10 consists of three parts: 1) a Rapid Load Testing Machine, 2) a control system, 3) a recording system. The design and construction of this equipment is described in reference (30). Briefly, the Rapid Load Testing Machine is a pneumatic-hydraulically operated mechanism designed to apply a constant tensile force rapidly to a specimen and to permit the rapid removal of the force on the specimen after a predetermined period of loading. The control system consists of suitable pressure regulators, pumps and additional plumbing which make possible the application of a predetermined force. The recording system consists of suitable power supplies, amplifiers and recording oscillographs to record the output of resistance sensitive strain gage bridges by which the force applied to and the strain in the specimen may be measured.

The original design of the Rapid Load Testing Machine used a hydraulic pressure differential across a piston to develop a force in the piston rod. The force was transmitted to the specimen through a rotation mechanism and a strain gage dynamometer. The rotation mechanism consisted of a pre-loaded axial bearing assembly and suitable attaching devices which permitted the rotation of the piston and piston rod with respect to the stationary dynamometer. The loading piston was rotated to reduce friction between the piston and cylinder walls by maintaining a continuous film of oil around the

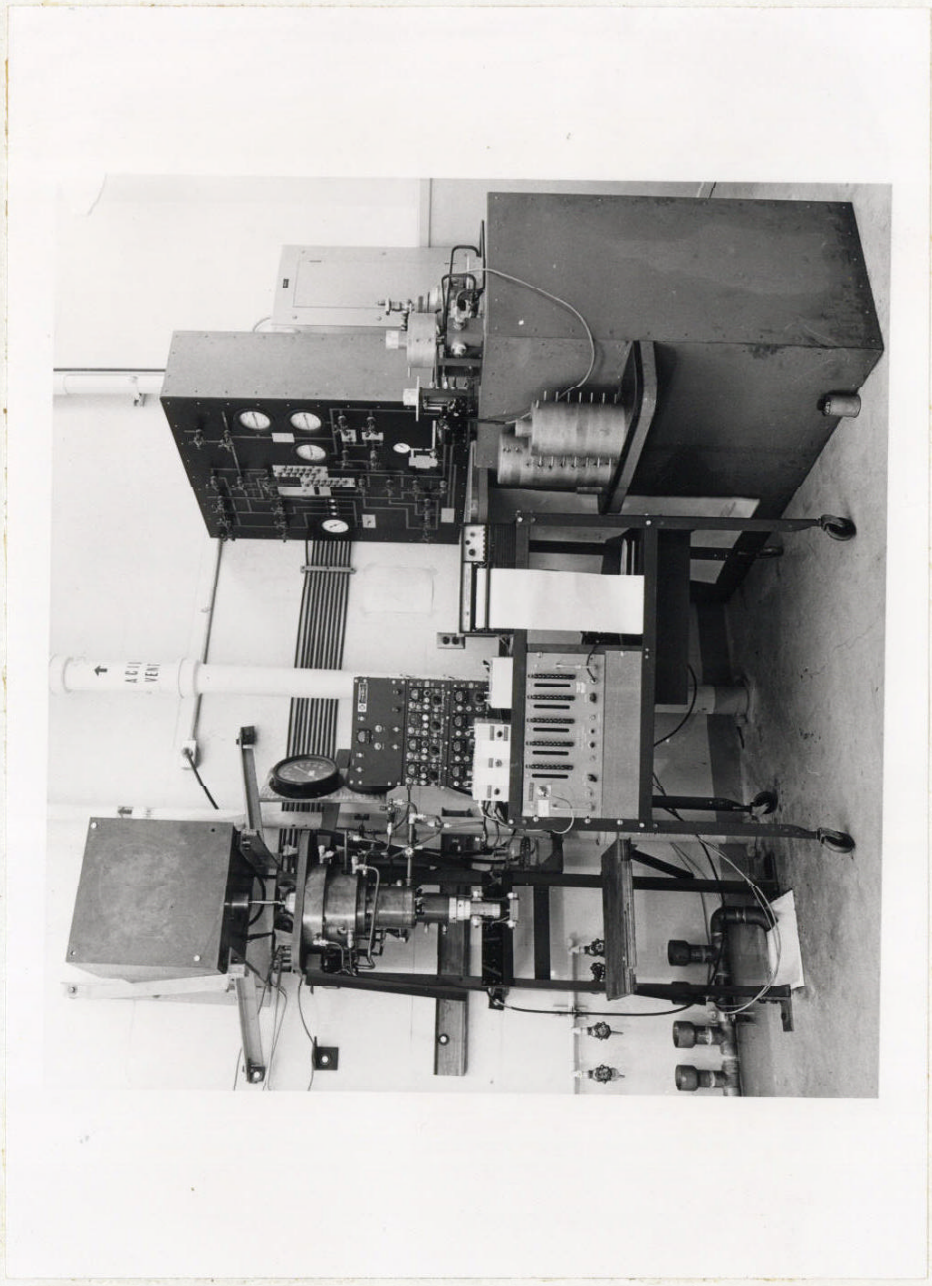

Fig. 10 General view of equipment for rapid load testing.

piston. The rotation mechanism caused two undesirable characteristics: 1) increased moving mass of the loading machine and 2) small oscillations of the load produced by the rotation mechanism. The Rapid Load Testing Machine was modified to eliminate the rotation mechanism, and to introduce an alternate method of maintaining a continuous oil film around the piston. The continuous film of oil is now maintained around the piston by controlled leakage. Areas of increased radial clearance were etched into the cylindrical surface of the piston. A continuous throttling rim at the top of the piston causes radial centering pressure forces to be developed when the piston is displaced from the center of the piston cylinder. The piston is attached to the piston rod through a spherical seat. This design provides a stable, self-centering piston which maintains a leakage path of uniform thickness around the piston. The modification eliminates the load oscillations and accomplishes a reduction in rise time by increasing the stiffness and reducing the moving mass of the loading system.

The Rapid Load Testing Machine applies the load to the specimen with a rise time of approximately 2×10^{-3} seconds, and maintains the load for preselected periods of $n \times 17 \times 10^{-3}$ seconds where n can be any integer between 1 and 100,000. The machine was designed for the application of a maximum force of 2000 pounds.

Loading Fixture

The loading fixture and its attachment to the Rapid Load Testing

Machine shown in figure 11 was designed to insure that the load axis would pass through the centroid of the specimen cross-section. Figure 12 is a photograph of the loading fixture parts. This fixture transmits equal forces to two parallel specimens. One specimen was made from heat treatable steel and was hardened so that its proportional limit was greater than the maximum stress to which the specimen would be subjected. The other specimen was the silicon-iron specimen which was to be tested.

Tests were conducted to determine the amount of bending in the test specimens. This was a final check on the specimen curvatures and the eccentricity of loading. Foil type strain gages were mounted on both sides of the test specimen and were connected in a Wheatstone bridge circuit to measure bending of the specimen. The force was applied to the specimen through the fixture by the use of an Instron testing machine.

Bending stress vs. applied load curves were obtained with the test specimen mounted 1) on the right side of the loading fixture, 2) on the left side, 3) on the right side with the specimen reversed (i.e., rotated 180° about is load axis) and 4) on the left side with the specimen reversed. The difference in bending stress induced by test (1) and test (2) above was twice the bending stress induced by the loading fixture. The sum of the bending stresses in test (1) and test (3) was twice the bending stress induced by initial curvature of the specimen. Test (4) was a check on the above results. The resultant bending stress due to initial curvature of the test

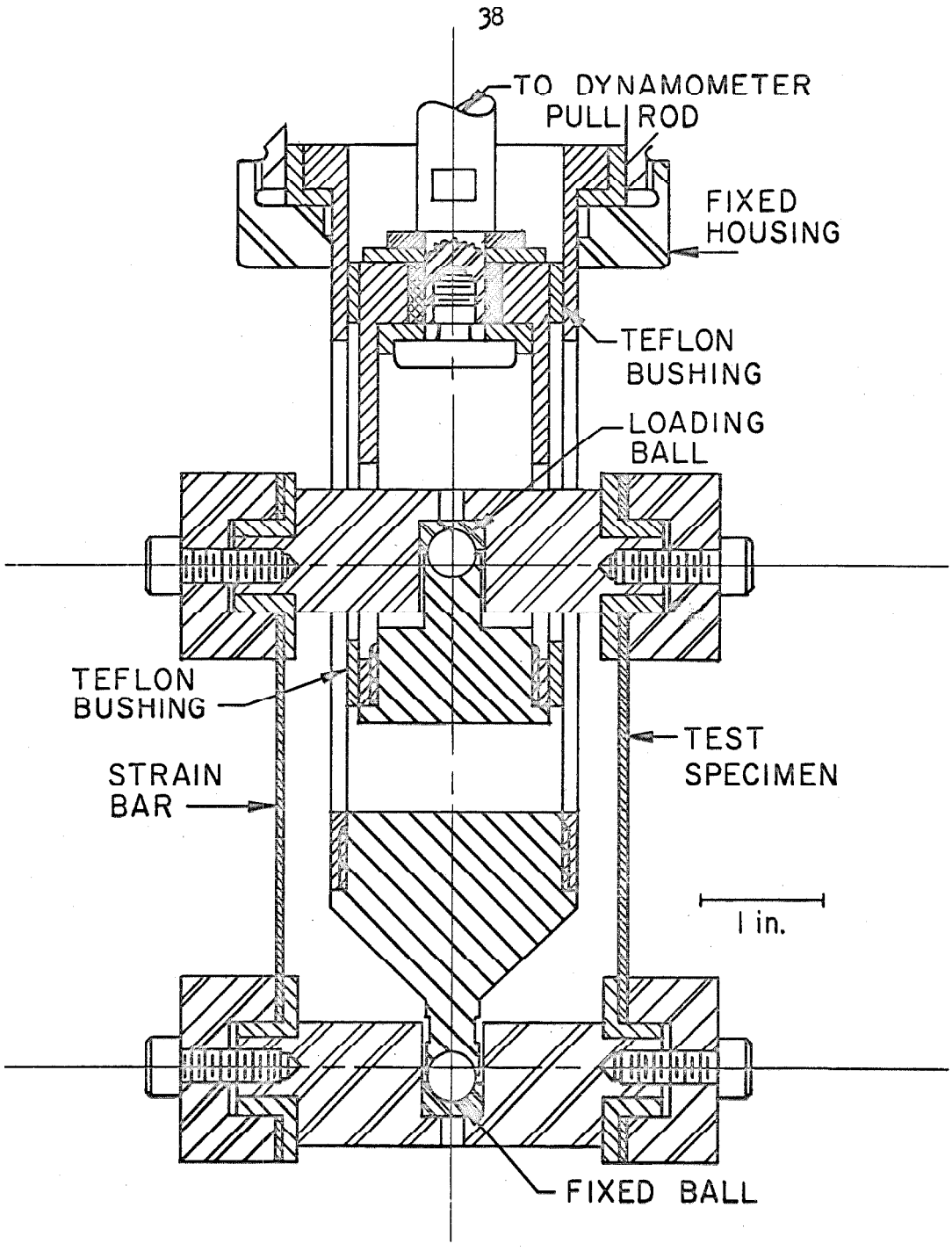

Fig. 11 Cross-section drawing of loading fixture for static and dynamic tests.

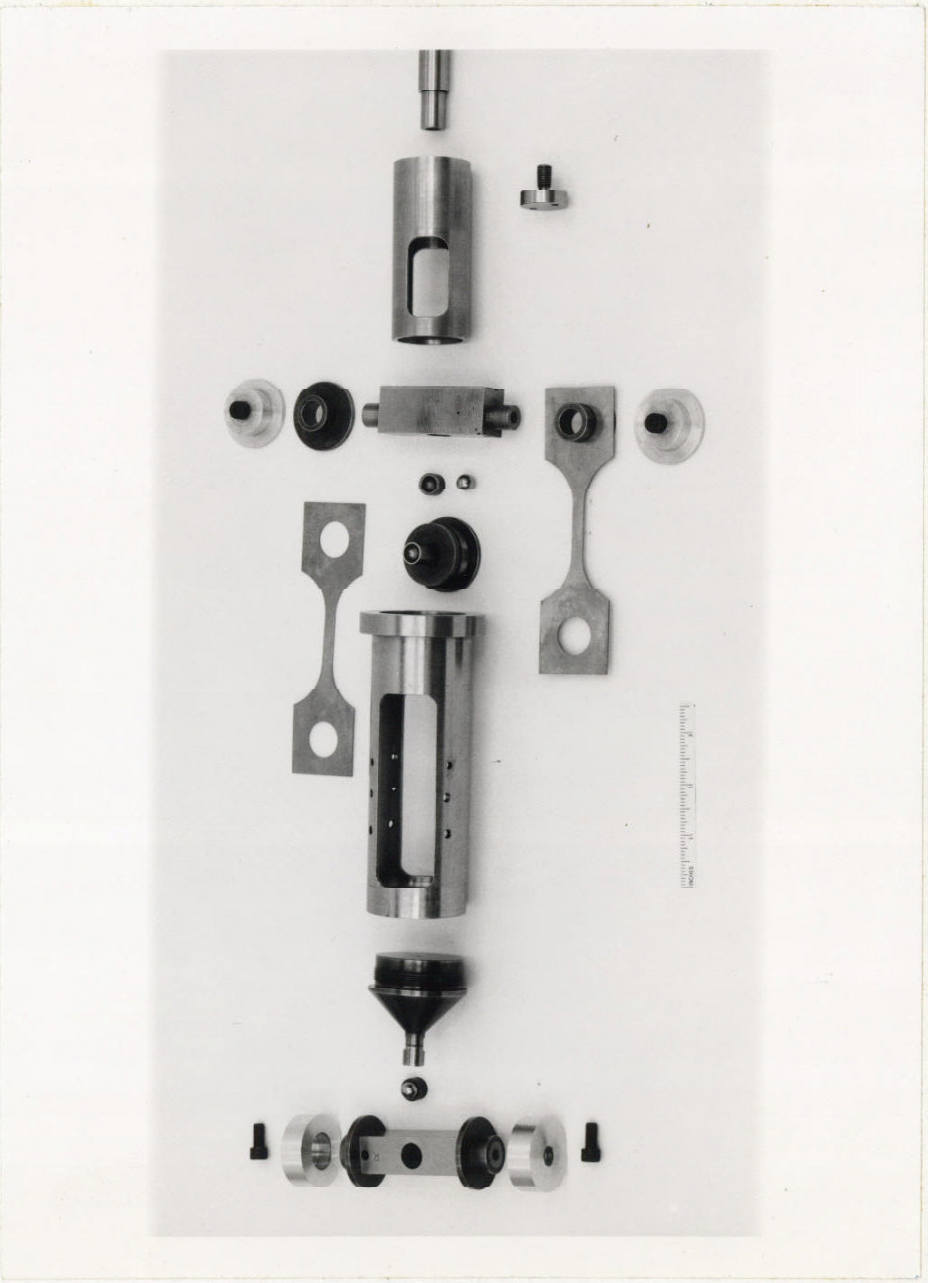

Fig. 12. Loading fixture parts. Compare with cross-section, figure 11.

specimen and non-symmetry of the loading fixture was less than one per cent of the tensile yield stress.

Load and Strain Measurements

The load acting on the specimen was measured by a strain gage dynamometer attached to the pull rod of the Rapid Load Testing Machine. The dynamometer was calibrated by harging known dead-weights directly on the pull rod in its assembled position and by recording the output of the dynamometer on the recording oscillograph. Prior to hanging the dead-weights on the pull rod, and again after removing the dead-weights, a fixed resistor of known value was switched into the Wheatstone bridge circuit parallel to one of the active gages and the deflection of the galvanometer trace produced by this resistor was recorded. The known value of "equivalent" bridge imbalance was then used as the calibration check prior to each test.

The strain in the specimen was detected by means of two foil type strain gages mounted on opposite sides of the gage section of the test specimen. The sum of the elastic and plastic strain in the specimens was not recorded. Only the plastic strain in the specimen was recorded. This measurement was accomplished by the use of gages on the heat treated specimen mounted parallel to the test specimen in the loading fixture. The heat treated specimen, or strain bar, had a proportional limit sufficiently high to insure that the strain in the strain bar accurately followed Hooke's Law. Two

strain gages of the same type as those used on the test specimen were mounted on the strain bar. The four gages on the specimen and strain bar were connected in a Wheatstone bridge circuit in such a way that the output signal was proportional to the difference between strains in the strain bar and in the specimen. The cross-section of the strain bar was such that the elastic strains in the specimen almost canceled those in the strain bar. This arrangement permits the use of the maximum possible sensitivity of the recording system without exceeding the total strain-recording capacity of the system.

The output of the strain gage bridges was amplified by means of type 1-113B, Consolidated Electrodynamics Strain Gage Amplifiers. The amplifier output was recorded on a Consolidated Electrodynamics direct writing oscillograph. The oscillograph galvanometers were type 7-315 which have a resonant frequency of 1,000 cycles/sec. The maximum sensitivity of the amplifiers in the strain measuring circuits could be used only when the elastic strain difference between specimen and strain bar was less than 0.00002 in./in. which corresponds to 0.1 per cent variation in test specimen cross-section. This close control of specimen geometry would have been too time consuming. An alternate method of achieving the maximum sensitivity of the strain measuring circuitry was to decrease the effective sensitivity of the gages on the strain bar (31). (See figure 13.) The effective elastic strain difference as measured by the amplified output signal from the bridge circuit could thus be reduced to approximately zero. The maximum sensitivity of the strain measuring

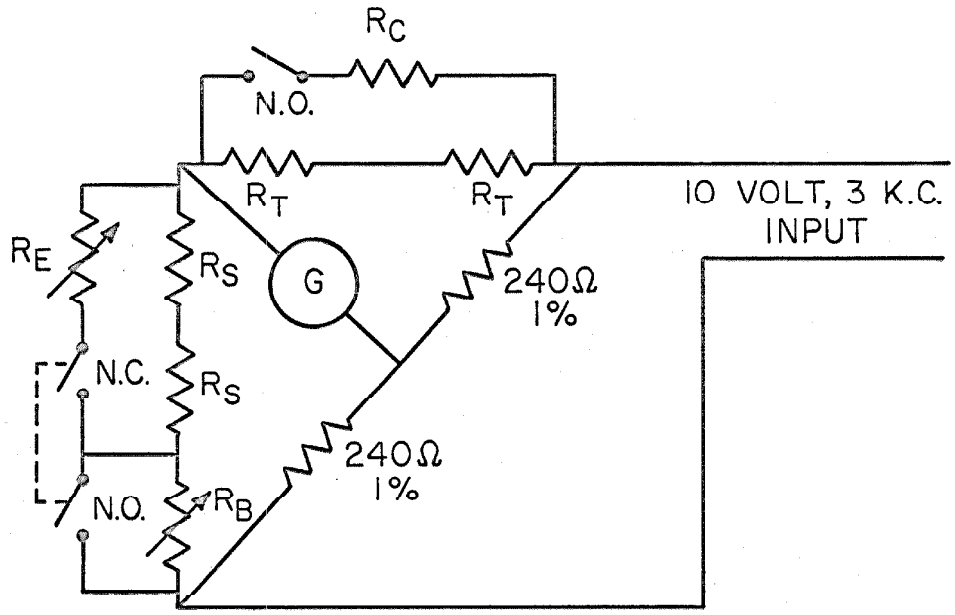

R_C = CALIBRATION RESISTOR

R_T = 120Ω TEST SPECIMEN GAGE

R_S = 120Ω STRAIN BAR GAGE

R_E = 2K TO 52K Ω GAGE FACTOR ADJUSTMENT

R_B = 0 TO 25Ω BRIDGE BALANCING RESISTOR

$$\epsilon_p = \frac{1}{G.F.}\left[\frac{R_T}{R_T + R_C/2}\right]$$

ϵ_p = PLASTIC STRAIN EQUIVALENT OF CALIBRATION RESISTOR.

G.F. = GAGE FACTOR OF FOIL STRAIN GAGES

Fig. 13 Plastic strain measuring circuit used in rapid load tests and static test measurements of microstrain.

circuitry was 20 x 10^{-6} in./in. per inch of trace deflection on the oscillograph recording paper.

Static Test Equipment

Static tests and constant strain-rate tests were made with a 10,000 pound Instron tensile testing machine. The loading fixture shown in figure 11 was adapted for use in the Instron as well as in the Rapid Load Testing Machine. A photograph showing the loading fixture and the Instron testing machine is shown in figure 14. The rod shown above the crosshead extended through the crosshead and was attached to the top of the specimen and strain bar through a spherical seat. Load was applied by moving the crosshead downward. The rod was loaded in tension and the force on the specimen was determined by means of the standard tension load cell on the Instron machine.

All test data for static tests and for constant strain-rate tests were recorded on the X-Y chart recorder on the Instron. The X-axis displacement of the recording pen was proportional to strain and the Y-axis displacement was proportional to load during stress-strain tests. Constant strain-rate tests were only conducted for the purpose of determining the Luder's band propagation velocity and Luder's strain. The recording pen was displaced in the X-direction proportional to crosshead displacement and in the Y-direction proportional to load. Luder's strain was proportional to the X-axis

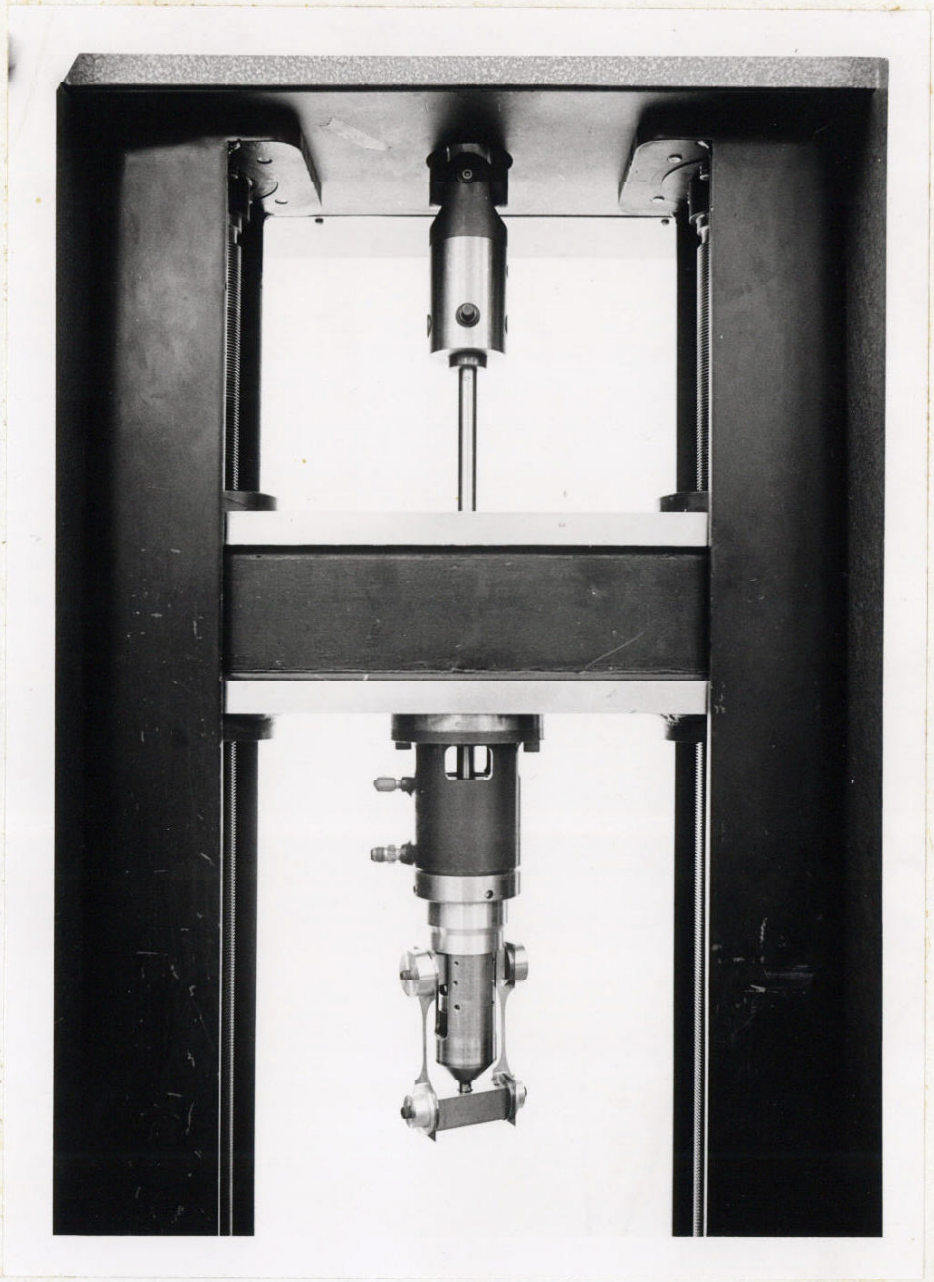

Fig. 14 Loading fixture adapted to Instron testing machine.

deflection since during Luder's band propagation the loading rate is zero.

Etch Pit Techniques

The change of dislocation configuration (density, distribution, shape, etc.) in a pulse loaded specimen may be observed by comparing a photomicrograph of the dislocation configuration prior to loading (initial configuration) with a photograph of the same area after the load has been applied and released (final configuration). The desirability of making these observations on that portion of the specimen directly under the strain gage which was used to record the plastic strain is obvious.

The electropolish and electroetch technique used by Dunn and Daniels (6) was employed in this investigation to reveal dislocation intersections with the observation surface. This electrolytic process uses a chrome-acetic acid electrolyte in which the specimen is the cathode. A technique was developed here to permit the determination of initial and final configurations after completion of mechanical testing.

The Dunn and Daniels etching technique for revealing dislocation sites in silicon-iron required that impurities segregate at the dislocation sites. These impurities are assumed to be carbon/and or nitrogen, since wet hydrogen treatment to remove carbon and nitrogen from the iron also removes the capacity to etch dislocation sites. All dislocations remaining in the material after the annealing treatment can be presumed to have the segregation required for the

formation of etch figures, if the carbon content in the specimen has been carefully controlled (27). Freshly formed dislocations in the annealed material will not have the segregated atmospheres at 75°F, and will not be revealed by the etching procedure. Subsequent aging at 320°F will allow impurities to diffuse to the fresh dislocation sites and thus allow them to be revealed by additional etching. The following procedure was developed to reveal the initial and final dislocation configurations in that portion of the gage section covered by strain gages:

1. Apply strain gages to finished specimen.
2. Conduct a stress-strain test.
3. Remove strain gages with suitable stripper at room temperature.
4. Polish and etch specimen to reveal initial configurations, take photomicrographs.
5. Age specimen for one hour at 320°F.
6. Etch specimen to reveal final configuration, take photomicrographs.

Internal dislocation configurations were studied by preparing sections through the specimen in that portion of the gage length directly under the strain gages. Both the initial and final dislocation configurations were observed after cutting the specimen at 45° to the tensile axis using an electric spark discharge machine and mounting the exposed section between stainless steel strips in "Quik-Mount", a room temperature curing plastic. These specimens were then abraded on metallographic papers to remove all spark damaged material prior to polishing and etching as described above in steps 4, 5 and 6.

Technique for Determining Orientation of Individual Grains in Polycrystalline Specimens

In order to determine the orientation of a grain with respect to the specimen surface, it is necessary to locate two poles. The procedure given by Barrett (32) was modified to permit use of existing laboratory equipment. An etchant was used to produce etch pits or facets with plane faces of low index. The plane faces thus revealed were $\{100\}$ planes in the case of 3 1/4 per cent silicon-iron, while those described by Barret are $\{100\}$ planes in α-iron.

The orientation with respect to the specimen surface of one $\{100\}$ pole was determined by obtaining a maximum intensity of the reflected light beam from a $\{100\}$ facet. The use of a highly collimated light source enhanced the accuracy of the technique. A Unitron Microgoniometer Microscope with a magnification of about 400 diameters was used for this orientation. The specimen stage of the microgoniometer rotates about the optical axis of the microscope tube when the tube is vertical. The tube of the microscope is mounted on a counterbalanced arm which pivots about a horizontal axis passing through the focal point of the objective lens. Thus it is possible to rotate the specimen stage and the microscope tube while maintaining focus on the specimen. The angles necessary to produce a maximum intensity reflection from a $\{100\}$ plane were plotted as a point on a stereographic projection. A piece of tracing paper was fastened over a stereographic net by a pin at the center of the net. Angles measured on the stage rotation circle correspond

directly to rotation of the tracing paper with respect to the stereographic net, while angles on the microscope tube circle correspond to angles to the right or left along the equator of the stereographic net. For convenient reference, the tensile axis of the specimen was made to coincide with the equator of the stereographic net when both of the above angles were zero. The basic circle of the net was the representation of the specimen surface and the center of the net represented the specimen surface normal. The physical construction of the Unitron Microgoniometer was such that it was impossible to obtain more than one $\{100\}$ pole for each grain in the polycrystalline specimen.

The second pole was obtained by observing the angle between the tensile axis of the specimen and the slip trace on the observation surface. The "locus of all plane poles" on a stereographic projection capable of producing a given slip trace on the surface of a specimen must be on a diameter at right angles to the observed slip trace. This principle was used to locate three possible $\{110\}$ poles which could represent the single slip trace observed. These three possible poles were determined by plotting points on the "locus of all plane poles" which were 45 and 90 degrees from the $\{100\}$ pole determined by use of the microgoniometer. For each of these possible $\{110\}$ poles, the resolved shear stresses on the $\{110\}\ \langle 111 \rangle$ slip systems were calculated. That orientation having the highest value of resolved shear stress on a $\{110\}\ \langle 111 \rangle$ slip system was assumed to be the correct orientation.

IV. TEST PROCEDURES

Two basic types of tests were conducted on the various specimens used in this investigation. Constant strain-rate tests were conducted to determine: a) the static stress-strain curves for polycrystalline and single crystal specimens and b) the velocity of propagation of Luder's bands in polycrystalline specimens. Rapidly applied constant stress pulse tests were conducted to determine: a) delay-times for yielding in fine grain polycrystalline specimens, b) dislocation velocities in individual grains within a polycrystalline specimen and c) dislocation velocities in single crystal specimens. The method of obtaining and recording data is described for each series of tests. All tests were conducted at room temperature of about 75°F.

Constant Strain-Rate Tests

A. Stress-Strain Curves

The loading fixture described in Part III was used for all static or low strain rate tests. This fixture was designed for the Rapid Load Testing Machine, but was adapted to the Instron testing machine and was used for both polycrystalline and single crystal specimens.

Constant strain-rate tests were conducted to determine the plastic strain vs. stress curves for fine grain polycrystalline specimens. One group of specimens was strained until the loading rate was almost zero, and then unloaded to permit determination of the residual microstrain. A second group of specimens was strained beyond the upper yield point strain where the loading rate became negative.

A total of nine fine grain polycrystalline specimens was strained in the above manner to determine the early portions of the static stress-strain relation with highest possible sensitivity. Seven specimens were strained at 0.010 in./min crosshead speed and two were strained at 0.020 in./min crosshead speed. Five of the specimens were strained beyond the yield point drop until work hardening caused the stress to increase again.

Several of the above polycrystalline specimens were polished and etched to reveal the dislocation configurations resulting from various amounts of pre-yield microstrain. Luder's bands had developed in some of these specimens. Photomicrographs were taken of the resulting dislocation configurations on the surfaces and cross-sections of the specimen. One static stress vs. engineering strain curve was obtained from a single crystal specimen, S1, and a few static stress vs. engineering strain curves were obtained from polycrystalline specimens. The total strain in each of these specimens was recorded. A two active-arm resistance strain gage bridge was used to determine the strain. The two remaining arms of the bridge circuit were temperature compensating gages of the same type as those used on the test specimen.

B. Luder's Band Front Velocity and Propagation Stress

The technique used for the production of single crystals required, as an intermediate step, the "critical" straining in tension of the fully annealed polycrystalline strips (28). The strips were strained

in the Instron at constant strain rates and the stress required to propagate a Luder's band at constant velocity was determined. The standard clamping jaws of the Instron were used to grip the strips. The clamping conditions initiated Luder's bands at each end of the specimen. These two band fronts then propagated toward the middle of the tensile strip at a constant velocity which was determined by the constant rate of elongation imposed by the crosshead.

The X-Y chart recorder on the Instron was used to record the load-time curve. The Y-axis displacement was proportional to load and the X-axis displacement was proportional to crosshead displacement. The X-axis of the recorder was driven at constant speed by a synchronous motor. The load on the specimen just prior to the meeting of the two Luder's fronts was used to determine the stress necessary to propagate the front at constant velocity.

The number of moving Luder's band fronts was determined by direct observation. Oblique illumination of the surface of the strip created a contrast pattern on the smooth surface. This contrast was due to the "orange peel" surface deformation associated with the Luder's band. There were always two fronts propagating into relatively unstrained material until they joined at the center of the specimen. Thirteen tests were conducted at various crosshead rates between the limits of 0.005 in./min and 2.0 in./min. The distance between the jaws on the Instron was 3.7 in. and the time required for the two moving Luder's band fronts to traverse this gage length was determined from the load-time curve. The specimen strain due to the

propagation of the Luder's band was determined by multiplying the propagation time by the crosshead speed. The machine compliance did not introduce errors in determining the Luder's strain by this method since the Luder's bands propagated at constant load.

Rapid Load Tests

A. Delay-Time in Fine Grain Polycrystalline Specimens

Rapid loading tests were made on fine grained silicon-iron specimens to ascertain if this material exhibited a delay-time for the initiation of catastrophic plastic deformation similar to that found for annealed low-carbon steel (13). The procedure used was similar to that reported previously by Clark, Wood and coworkers (13, 18).

The specimen with strain gages attached was mounted in the loading fixture and the gages were connected as shown in figure 13. The recorded signal was proportional to the strain in the specimen minus the elastic strain in the strain bar. Hydraulic pressures were adjusted to apply a preload of approximately 10 per cent of the lower yield stress to the specimen. The difference in elastic deformation between the strain bar and test specimen caused the bridge circuit of figure 13 to become unbalanced. The variable resistors R_B and R_E were then adjusted to give a slight negative imbalance of the bridge with respect to the imbalance caused by plastic deformation of the test specimen. The stiffness of the strain bar was slightly less than the stiffness of any of the test specimens, since this is required for the above procedure to be effective. Then when the test is performed, the

transition from elastic to plastic deformation in the test specimen causes a sharp transition in the rate of strain difference from a slightly negative rate to a sharply positive rate.

Prior to the test, the preload was removed so that the bottom ball of the loading fixture was free from its seat. At this point the "zero" load on the specimen and the calibration for the load dynamometer and strain measuring circuit were recorded on the recording oscillograph by manual activation of the oscillograph and calibration switches. The hydraulic pressures were again adjusted to apply a slight preload to the specimen. The preload eliminated all clearances in the loading mechanism between the actuating piston and the specimen. This preload also corresponded to less than 10 per cent of the nominal lower yield stress of the specimen and permitted the optimum rise time for the rapid loading pulse. The recording oscillograph was started before the application of the square wave load pulse to allow the recording paper to reach full speed before load application. The duration of the rapid load pulse and running time for the recording paper were preselected and initiated in the proper sequence by use of suitable relays and timing circuits. A second "zero" and calibration record was made after the test to see that no drift or failure of the load measuring circuitry had occurred during the load pulse. The entire sequence required less than one minute total elapsed time, and thereby minimized errors due to changes in hydraulic pressures, temperatures of recording devices and line voltage variation during the test.

Delay-time tests were conducted on ten fine grain polycrystalline specimens at stresses of 71,500 lb/in.^{2} to 75,500 lb/in.^{2}. One objective of these delay tests was to observe the dislocation configurations associated with various stages of development of the pre-yield plastic microstrain.

B. Dislocation Velocity Tests in Polycrystalline Specimens

Dislocation velocity determinations were only made on coarse grain polycrystalline specimens because of experimental difficulties encountered in determining the orientation of individual grains within the fine grain specimens. Rapid loading stress pulses were used to cause fresh dislocations to propagate within a single grain. The average propagation velocity was determined by dividing the length of the longest slip line within a grain, which did not terminate at a grain boundary, by the duration of the loading pulse.

Each specimen was lightly abraded with 600A silicon-carbide paper to remove any oxide or scale which had formed during the specimen preparation. The specimen was then electrolytically polished to remove all cold worked material. A source of fresh dislocations was introduced by scratching the polished surface with a conical diamond stylus (9). The load on the stylus was 3.6 grams. The elapsed time between scratching and pulse loading of the test specimen was less than 5 minutes which prevented immobilization of the fresh dislocations by diffusion of impurities to them.

The specimen was pulse loaded, aged for one hour at 320°F to decorate the dislocations and electrolytically etched to reveal the

dislocation configurations (6). Photomicrographs were then taken of those configurations from which data could be obtained. The grains in the photomicrographs with slip lines originating at the scratch and terminating within the same grain were numbered for reference purposes. The orientation of each numbered grain was then determined by the procedure given in Part III.

Four specimens were tested at tensile stresses of 50,100 to 59,400 lb/in.^{2} and loading pulse durations of 0.017 to 1.85 seconds. From photomicrographs of these specimens, 48 numbered grains were selected for analysis.

C. Dislocation Velocity Tests in Single Crystals

Rapid loading tests were conducted on freshly scratched single crystals to determine the stress dependence of the velocity of mobile dislocations. The orientation of the single crystals was determined by the back-reflection Laue X-ray diffraction technique prior to pulse loading. Multiple tests were possible on the single crystal specimens because aging of the specimens after each load pulse anchored all fresh dislocations. These aged dislocations did not act as sources for slip lines during subsequent tests.

Each specimen was abraded with 600A silicon-carbide paper, electropolished, scratched and pulse loaded in the same manner as the polycrystalline specimens above. After aging and electroetching, the length of the longest slip lines originating from the fresh scratch was determined by direct measurement using a filar eyepiece on a

standard metallurgical microscope. The average dislocation velocity was determined by dividing the observed length of the slip lines by the load pulse duration. After each velocity determination, the specimen was scratched again on an area of the gage section which did not contain slip lines from previous scratches, and pulse loaded again at a higher load to obtain another velocity determination. This procedure was continued until the gage section was covered with slip lines, or until the specimen failed by twinning.

Four single crystals were used to obtain nine velocity determinations over a range of velocities from 7.19×10^{-6} to 2.80×10^{-2} cm/sec. The corresponding resolved shear stress range was from 21,300 to 28,000 lb/in.^{2}.

V. EXPERIMENTAL RESULTS

Constant Strain Rate Tests

A. Stress-Strain Curves - Polycrystalline Specimens

Static stress-strain curves were obtained by the use of the Instron static testing equipment shown in figure 14. Typical stress-strain curves for polycrystalline specimens are shown in figure 15, and the results obtained from static testing data for fine grain polycrystalline specimens are summarized in Table 1. All polycrystalline specimens tested statically exhibited both an upper yield point and a lower yield point. The design of the loading fixture precluded straining to large values of plastic strain. The strain rate during plastic flow was much greater than the initial elastic strain rate because during elastic loading a substantial portion of the crosshead motion is related to the elastic deflection of the machine, the loading fixture, the pull rod, etc.

Typical stress vs. plastic strain curves for fine grain polycrystalline specimens M36 and M27 are shown in figure 16. Specimen M36 was strained until the loading rate was almost zero, and then unloaded to determine the residual microstrain. The plastic microstrain was determined by use of strain gages connected in bridge circuits as shown in figure 13. The initial slope of the curve for specimen M36 is due to the difference in elastic strain between the specimen and strain bar. The plastic microstrain at load is shown on the curve.

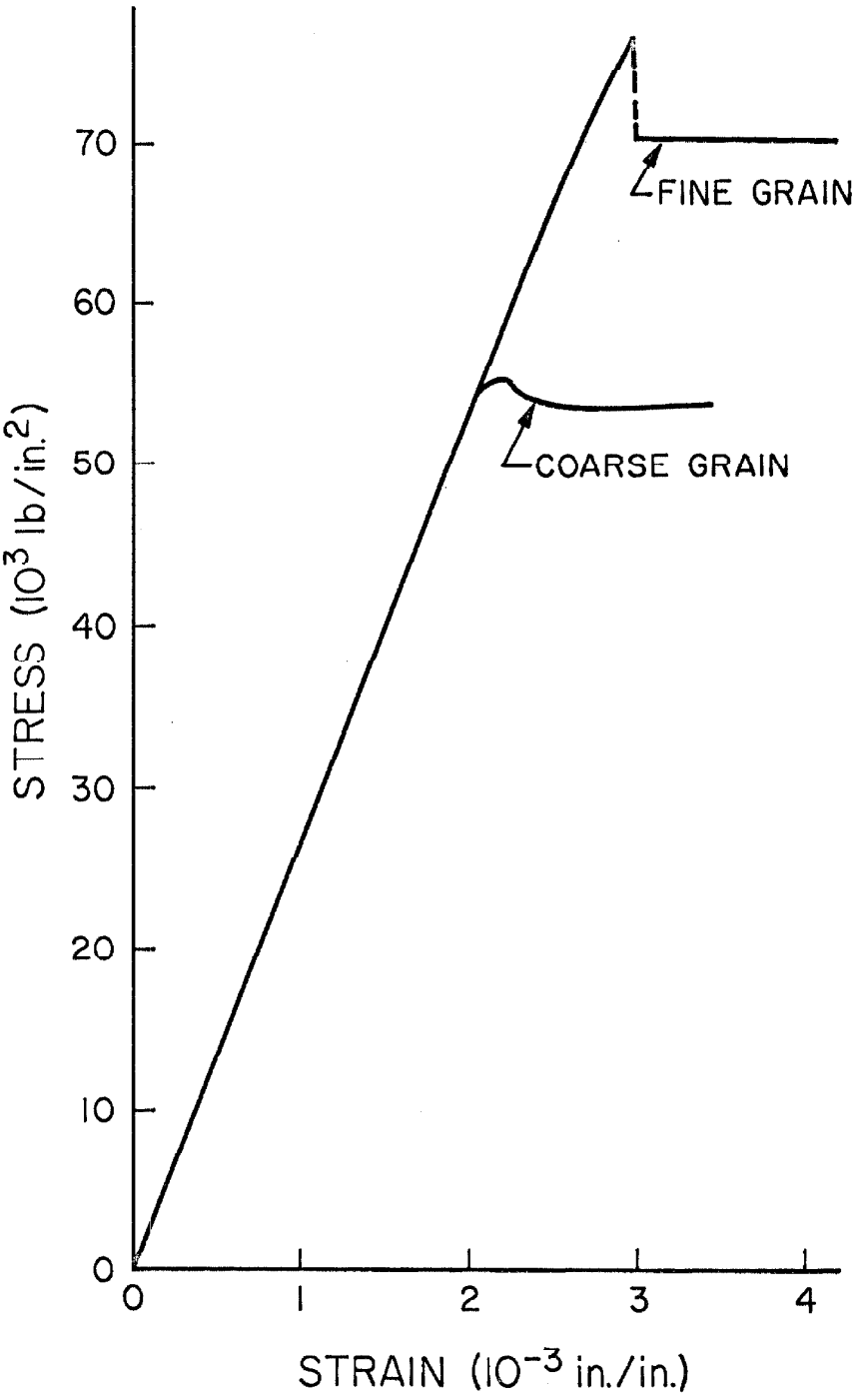

Fig. 15 Typical stress-strain curves for polycrystalline specimens. Average E = 26.8 x 10^6 lb/in.^{2}. Crosshead speed on Instron--0.010 in./min.

TABLE 1

Polycrystalline Stress-Strain Data
Fine Grain Specimens

Specimen No.	Crosshead Speed	Upper Yield Stress	Lower Yield Stress	Pre-Yield Microstrain at Upper Yield Point
	in./min	lb/in.^{2}	lb/in.^{2}	10^{-6} in./in.
M3	0.01	74,200	68,500	134
M5	0.01	76,600	70,200	97
M11	0.02	73,700	68,500	--
M12	0.02	71,600	67,100	--
M27	0.01	73,000	---	280
M28	0.01	75,100	71,200	44
M34	0.01	70,100	---	64
M36	0.01	71,500	---	118
M38	0.01	71,300	---	68

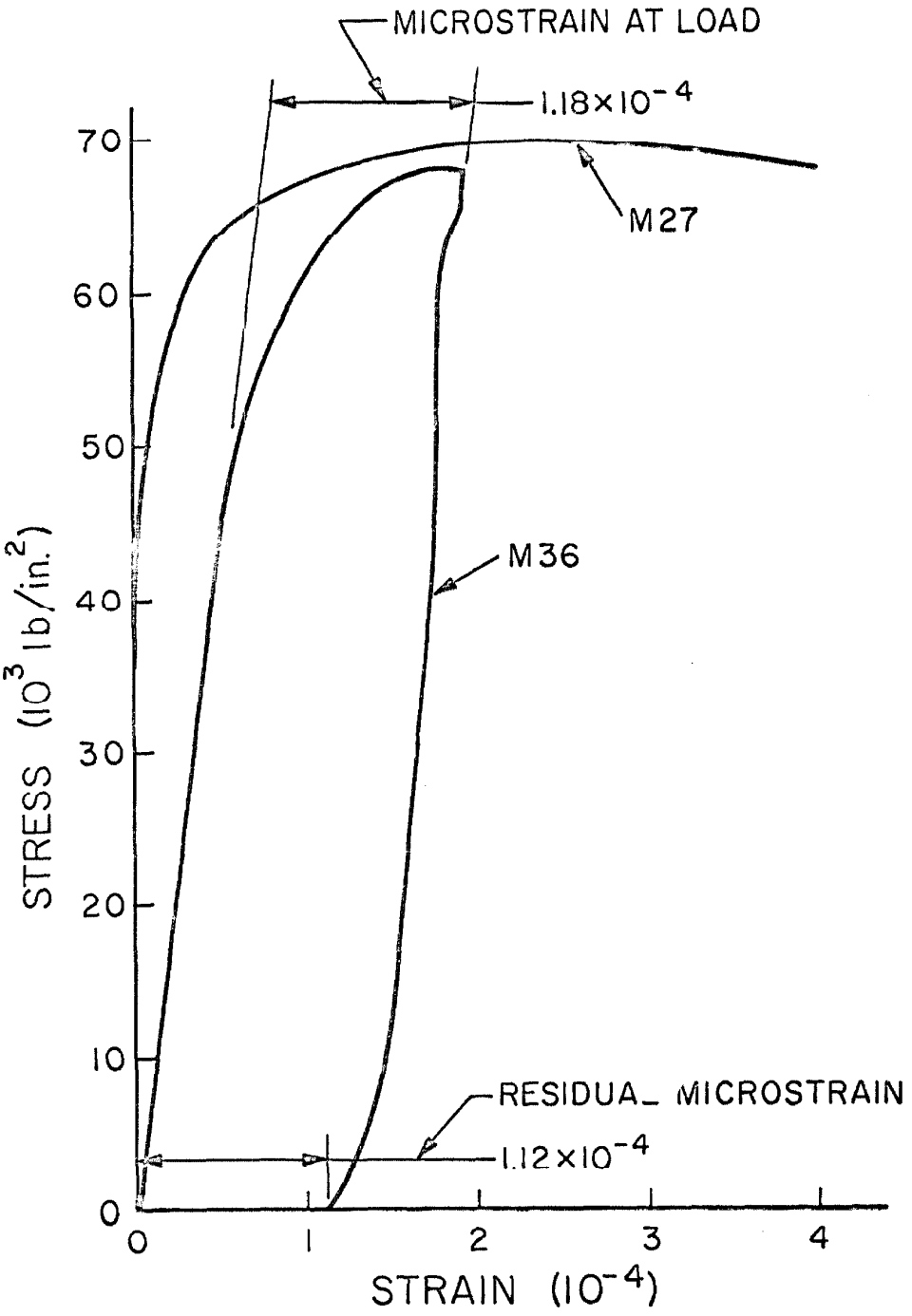

Fig. 16 Reproduction of typical stress vs. plastic strain record for fine grain polycrystalline specimens. Crosshead speed on Instron--0.010 in./min.

Specimen M27 was strained beyond the upper yield point. The stress on the specimen can be seen to decrease for strains greater than 280 x 10^{-6} plastic strain. The average strain under the strain gage can be seen to increase continuously as the total specimen strain increases. The upper yield point microstrain at load is about 280 x 10^{-6}.

B. Stress-Strain Curves - Single Crystal Specimen

Figure 17 is a static stress-strain curve of single crystal specimen S1. The location of the tensile axis for this specimen is shown on the unit stereographic triangle in figure 9. The yield point drop observed in this specimen was not due to lattice rotation as described by Barrett (33). Lattice rotation due to single slip always rotates the slip direction towards the tensile axis along a great circle on the stereographic triangle. The lattice rotation is related to the elongation by

$$\sin \phi_1 = (l_0/l_1) \sin \phi_0 \qquad (9)$$

where

ϕ_0 and ϕ_1 are the initial and final angles between the slip plane and the tensile axis,

and

l_0 and l_1 are the initial and final gage lengths, respectively (33).

From figure 17 it may be seen that the stress dropped from 57,000 to 55,000 lb/in.^{2} while the specimen experienced 375 x 10^{-6} in./in. of plastic deformation. The corresponding

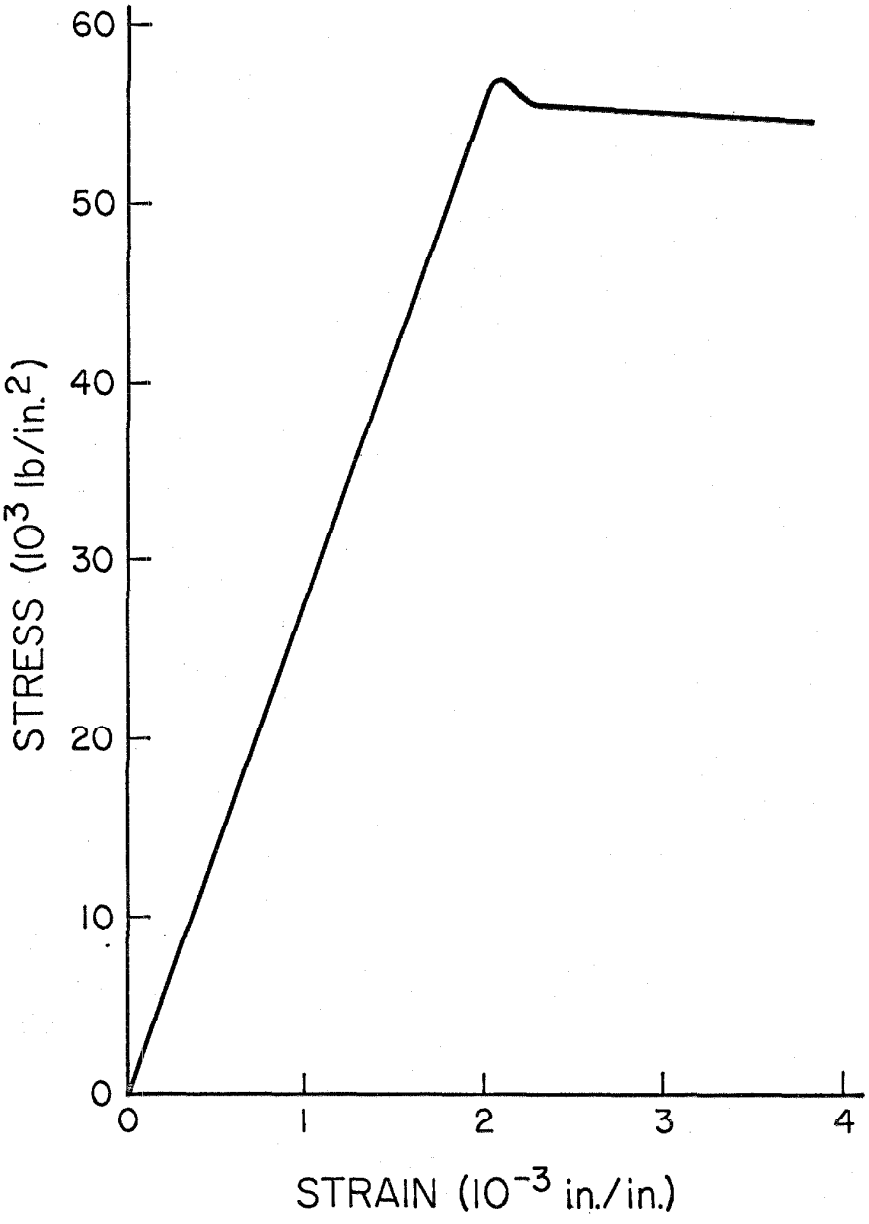

Fig. 17 Stress-strain curve for single crystal specimen S1. Crosshead speed on Instron--0.010 in./min. Schmid factor--0.467

resolved shear stress on the active slip system changed from 26,600 to 25,800 lb/in.^{2} and the angle change obtained from equation 9 is less than 10 seconds of arc. The reduction of resolved shear stress due to lattice rotation in this case would be no more than 10 lb/in.^{2} based on the Schmid equation

$$\tau_r = \sigma \cos\phi \cos\lambda \qquad (10)$$

where ϕ is the angle between the tensile axis and the normal to the slip plane, and λ is the angle between the tensile axis and the slip direction.

C. Luder's Band Front Velocities and Propagation Stresses

The stress necessary to propagate a Luder's band at constant velocity in polycrystalline 3 per cent silicon-iron alloy ($\bar{d} \approx 0.002$ in.) was determined by varying the crosshead speed on the Instron testing machine and observing the velocity of the Luder's band front. The total plastic strain in the specimen was determined by observing the time required to propagate the Luder's band front from the end of the specimen to the center. The motion of the crosshead corresponded exactly to the elongation due to strain, e_p, in the specimen since this strain occurred at constant stress. In all cases, there were two band fronts approaching each other so that

$$V_B = V_{CS}/2\epsilon_p \qquad (11)$$

where V_B is the Luder's band front velocity and V_{CS} is the cross-head speed. Table 2 gives the results for thirteen tests. Figure 18 is a representative load-time curve for specimen 1.

Figure 19 is a plot of the Luder's band propagation stress vs. the propagation velocity. The straight line curve was obtained by the "two-point" curve fitting technique. The data in Table 2 were divided into two groups. The seven lowest velocity tests formed one group and the remainder formed the second group. The average value of the lower yield stress and of the $\log_{10}(10 \times V_B)$ was calculated for each group. A straight line was drawn between the two "average" points determined for the two groupings. The analysis of the data relating to this curve will be given in Part VI.

The strain distribution associated with Luder's bands was observed by the use of etch pitting of dislocations. Luder's bands which developed during testing extended across the surfaces of the specimens. The band fronts were straight and parallel within $\pm$ 2 grain diameters and probably contained a large majority of the moving dislocations responsible for the Luder's strain. In the area ahead of the moving Luder's band front and within 10 grain diameters, 15 per cent of all grains on the surface of specimen M36 contained active slip systems as evidenced by slip traces within individual grains. These slip lines were all confined to one grain and did not penetrate any grain boundaries. The region immediately behind the moving front revealed that all grains had undergone extensive slip. The density of dislocations in all grains within the Luder's band

TABLE 2

Results of Luder's Band Velocity Tests
Polycrystalline Specimens

Specimen No.	Crosshead Speed	Total Plastic Strain	Lower Yield Stress	Band Velocity
	in./min	per cent	lb/in.^{2}	in./min
1	0.020	2.99	63,800	0.345
2	0.005	2.69	61,300	0.093
3	0.010	2.72	62,700	0.183
4	0.200	3.75	66,700	2.66
5	0.100	3.05	65,500	1.64
6	0.050	3.04	64,100	0.810
7	0.500	2.74	66,500	9.12
8	1.000	3.48	66,600	14.4
9	2.000	3.75	67,700	26.7
10	0.500	3.50	65,200	7.15
11	0.200	3.34	64,300	3.00
12	0.100	3.03	64,900	1.65
13	0.050	3.06	63,500	0.819

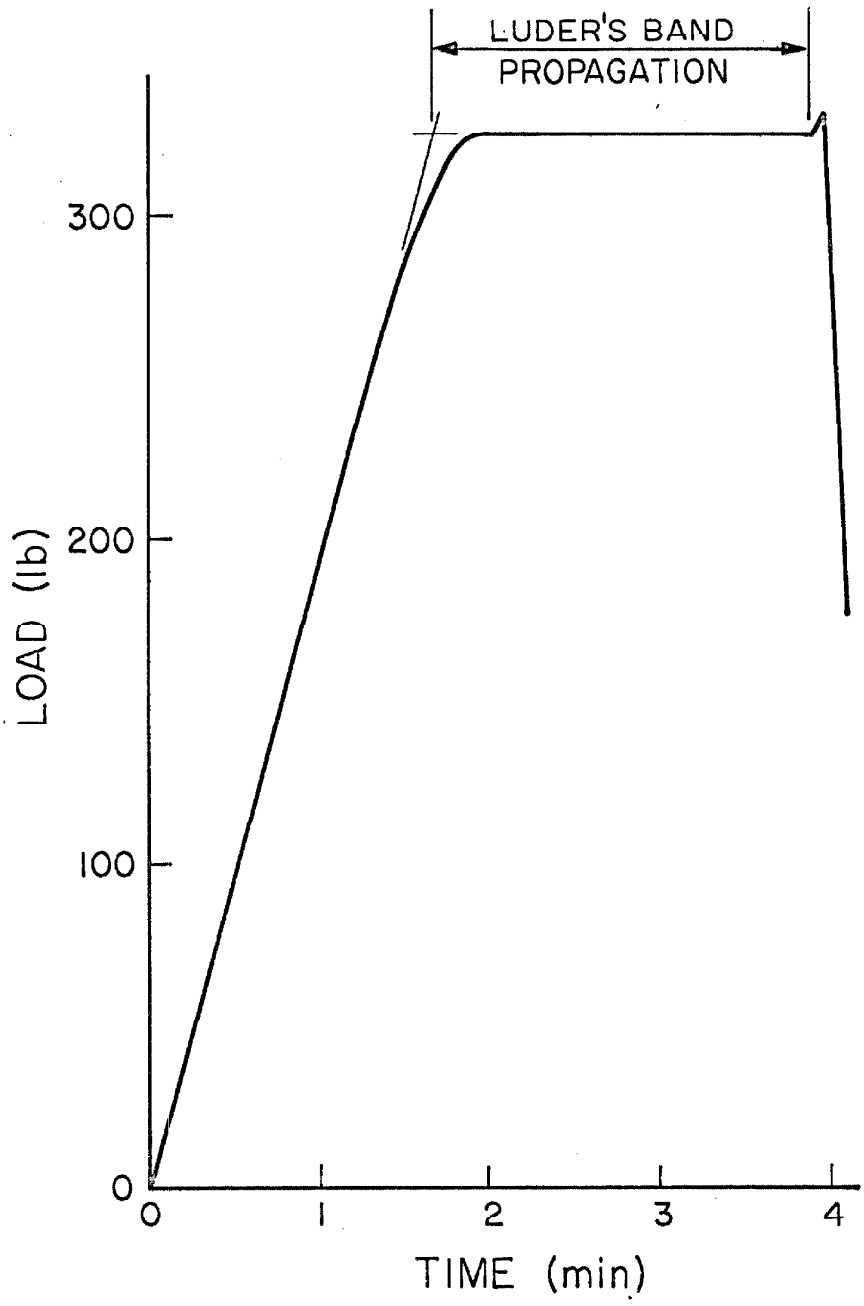

Fig. 18 Typical load-time curve for determining Luder's stress and strain. Specimen 1.

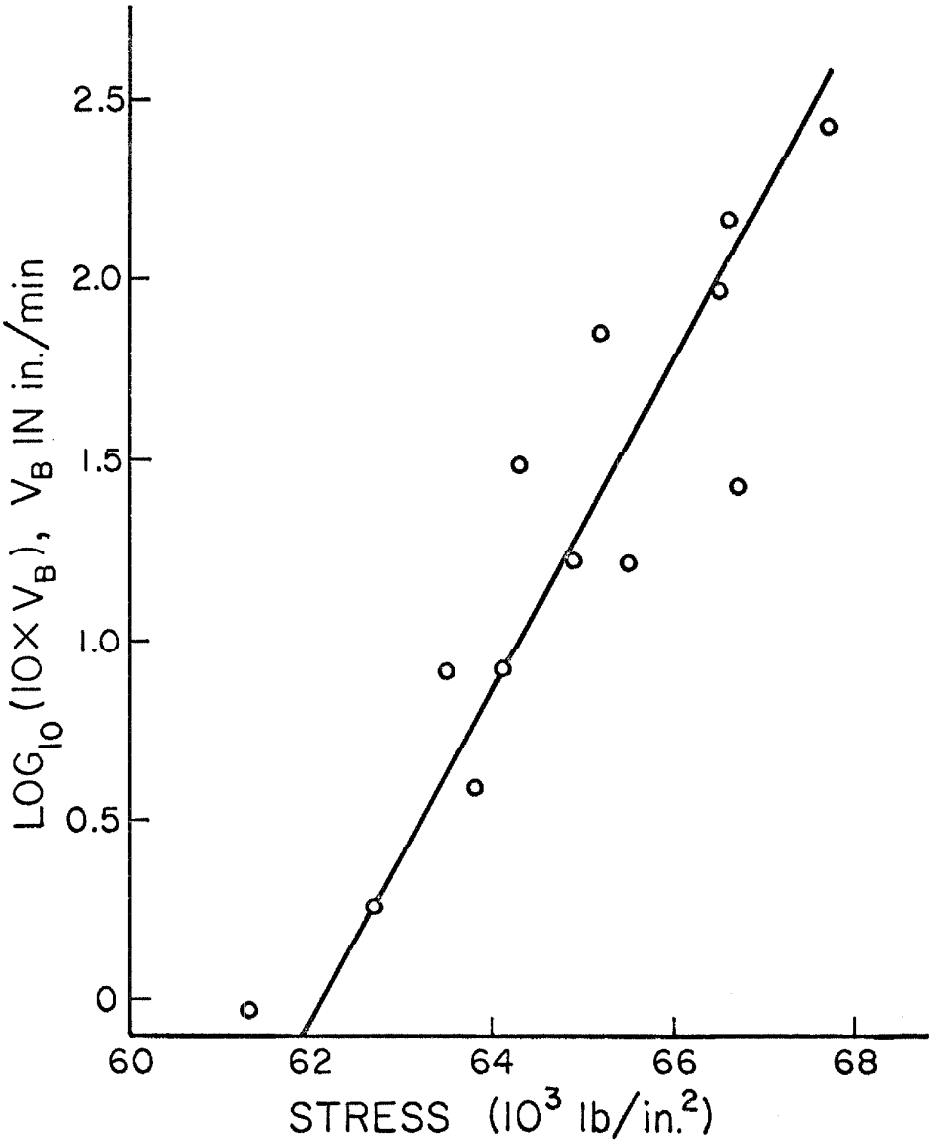

Fig. 19 Luder's band propagation velocity vs. stress.

was too high to identify any slip lines or families of slip lines at 1000X magnification.

Figure 20 is a photomicrograph showing the Luder's band front in specimen M36. This statically loaded specimen contained a Luder's band away from the strain gages. The residual microstrain recorded by the strain gages on specimen M36 was 112 x 10^{-6} in./in. after unloading, and the dislocation etch pit analysis revealed a total of 8.2 per cent of all surface grains under the gages contained active slip systems. Comparison of the three regions (the Luder's band front, within 10 grain diameters and under the gages) reveals that the transition between the material with the Luder's strain and the material with only a small fraction of yielded grains is confined to a linear region of approximately four grain diameters or 10^{-2} cm for the specimen shown.

Rapid Load Tests

A. Delay-Time in Fine Grain Polycrystalline Specimens

The silicon-iron used in this investigation exhibits a delay-time for yielding similar to that reported for low-carbon steel when subjected to a constant, rapidly applied stress (3, 13, 18). The addition of 3 per cent silicon to low-carbon steel increases the stress for a given delay time. For delay-times of the order of 10^{-1} seconds in specimens of comparable grain size, the stress increase is approximately 20,000 lb/in.^{2}, i.e., from 50,000 to 70,000 lb/in.^{2}.

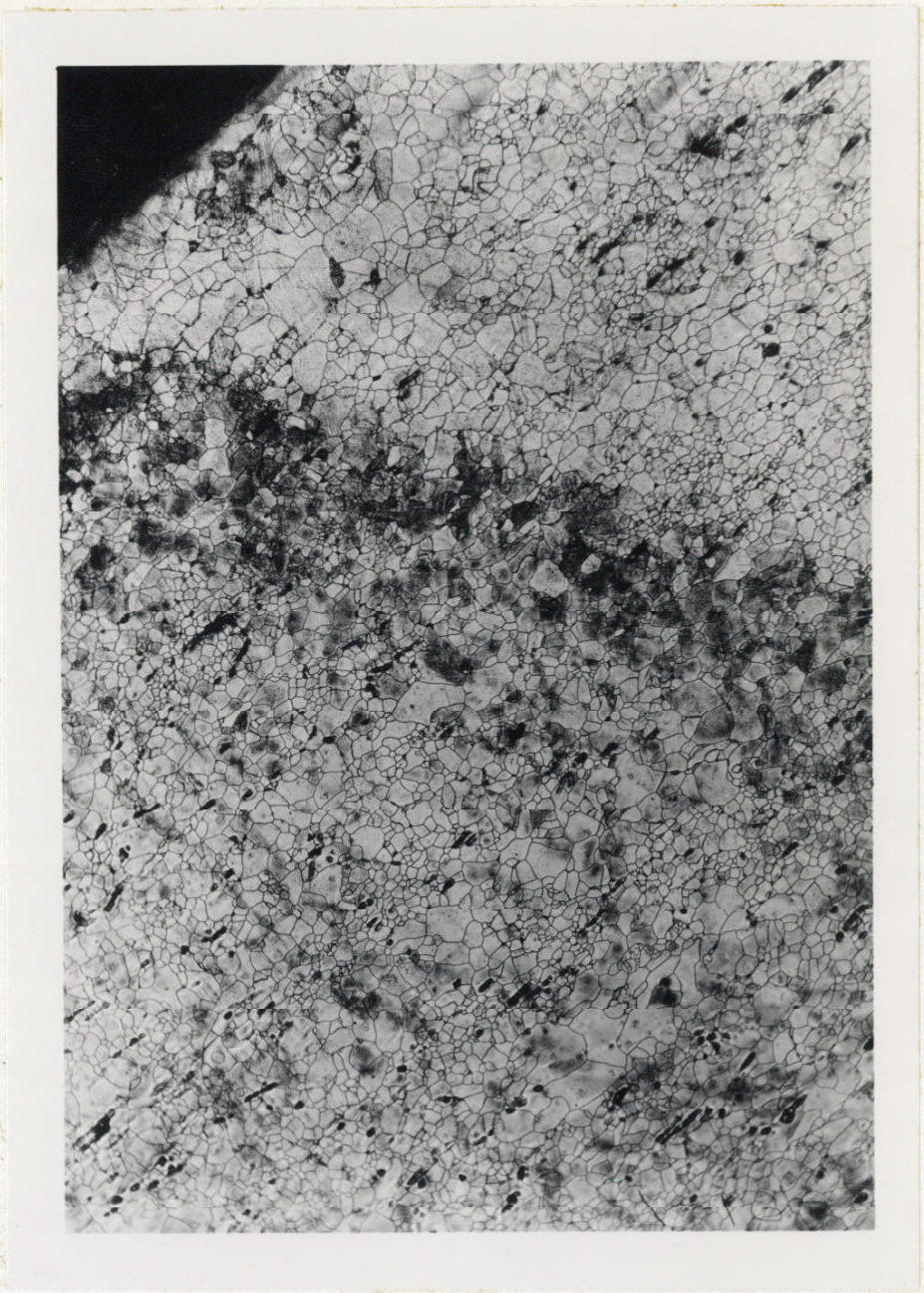

Fig. 20 Luder's band front in specimen M36. Etched to reveal dislocation sites. 100X.

A reproduction of a typical oscillograph record of the applied load and the strain vs. time is shown in figure 21. The delay-time for the initiation of yielding as shown for specimen M21 was 30×10^{-3} sec. The pre-yield plastic microstrain at the end of the delay-time was 140×10^{-6}. The delay-time as shown represents the initiation of the very rapid increase in strain rate which precedes the development of a Luder's band. The high sensitivity of the strain measuring device reveals the continuous nature of the growth of an embryonic Luder's band when the strain detected is the average value on a surface area 3/16 by 3/16 in. (i.e., gage dimensions). Luder's strain had not occurred under a significant fraction of the gage when the strain trace reached the edge of the recording paper. The load drop recorded for specimen M21 indicates that the strain rate of the specimen increased until the Rapid Load Testing Machine was no longer capable of maintaining the applied load at the required extension rate. Table 3 contains the results of nine delay-time tests on fine grain polycrystalline specimens.

Figures 22 and 23 are photomicrographs of a cross-section of a pulse loaded specimen etched to reveal dislocation intersections with the observation surface. The darker grains have a greater dislocation density than the lighter grains. In fact the lighter grains have not yet yielded. Figure 22 shows several relaxed grains clustered together to form a relaxed nucleus of yielding within the bulk of the specimen. Figure 23 shows a different portion of the same cross-section in which the nucleus of yielding has spread through

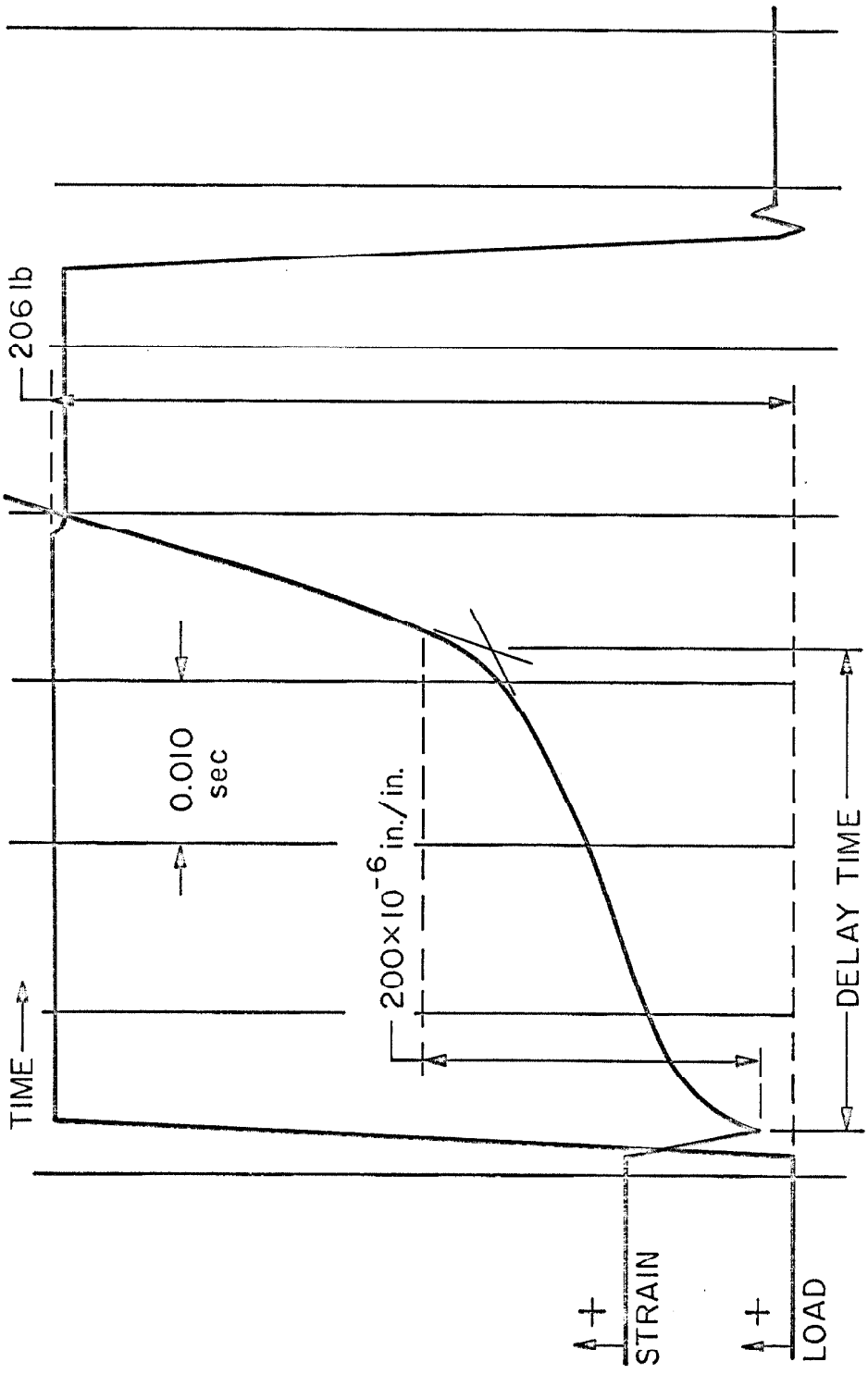

Fig. 21 Reproduction of rapid load testing record for specimen M21.

TABLE 3

Results of Delay-Time Tests at 75°F
Fine Grain Polycrystalline Specimens

Specimen No.	Applied Stress $lb/in.^2$	Delay-Time sec	Pre-yield Microstrain 10^{-6}
M15	75,500	0.050+	168
M17	72,300	0.050	112
M21	73,300	0.036	140
M22	72,400	0.015	158
M23	72,500	0.050+	153
M24	71,500	0.010	70
M39	74,600	0.170	--
M40	73,600	0.250	267
M43	72,700	0.263	165

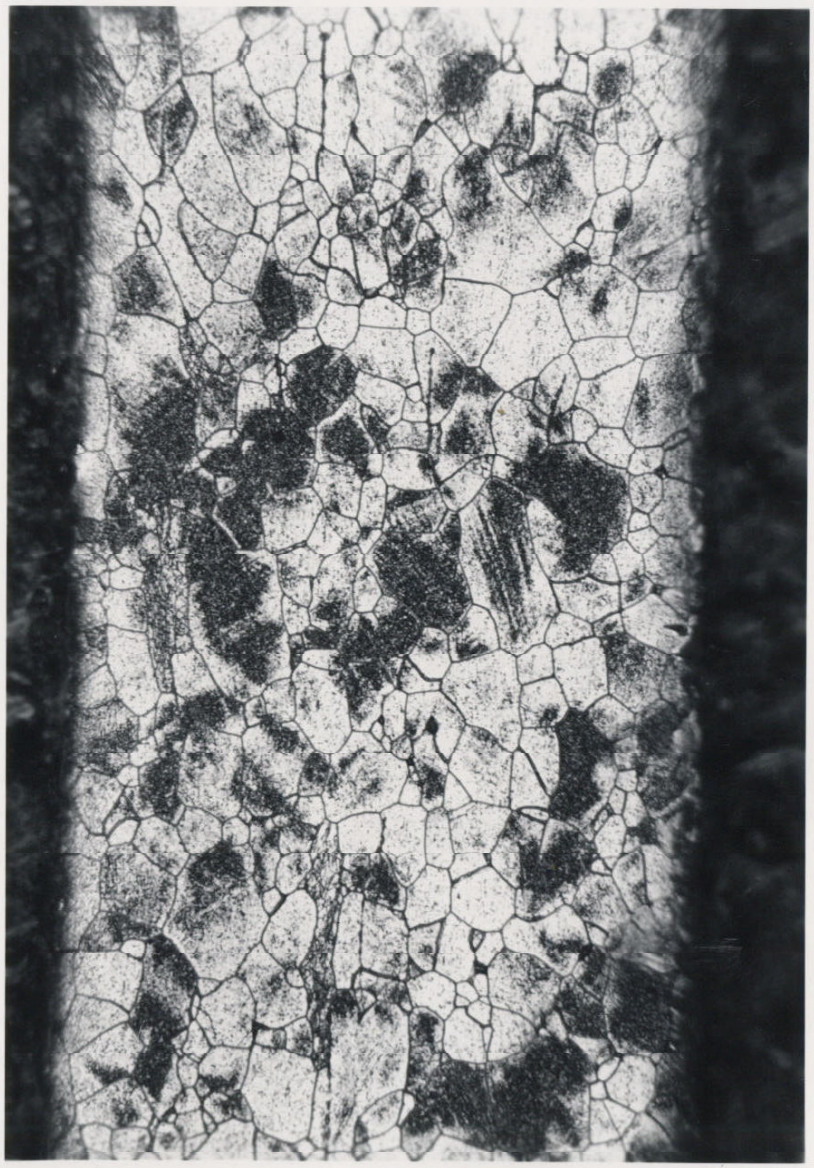

Fig. 22 Cross-section of specimen M21 prior to formation of a Luder's band. Etched to reveal dislocation sites. Dark grains--high dislocation density. 300X.

Fig. 23 Cross-section of specimen M21 showing an embryonic Luder's band. Etched to reveal dislocation sites. Dark grains--high dislocation density. 300X.

the thickness of the specimen to both free surfaces.

B. Dislocation Velocity Tests in Polycrystalline Specimens

The results of the polycrystalline stress vs. dislocation velocity tests are presented in Table 4. The resolved shear stress given in the table was calculated on the assumption that a $\{110\}\ \langle 111\rangle$ slip system was active during deformation. The curve shown in figure 24 is a "best" fit of the stress vs. dislocation velocity data to equation 7. Data from grains number 3, 4, 8 and 12 in specimen T3; 7 in specimen T8; and 4 and 9 in specimen T16 were discarded, and the remainder of the data was divided into two groups. The discarded grains were judged to be erroneous because of large values of standard deviation from the "best" fit curve for the data. Grains in specimens T3, T8 and T2 formed one grouping and grains in specimen T16 formed a second grouping. These groups were used as the basis for a "two-point" best fit curve. This curve fitting method gave a lower value of standard deviation than a "least squares" fit.

Photomicrographs of typical dislocation configurations obtained from pulse loaded coarse grain polycrystalline specimens are shown in figures 25 and 26. The fresh dislocations produced by the central scratch act as sources for dislocation slip lines, and produce far greater numbers of slip lines than any other sources in the specimen.

Figure 27 is a composite of six selected areas of photomicrographs which illustrate the relaxation process in individual grains. The growth of a slip band appears to occur by the addition of

TABLE 4

Results of Polycrystalline
Stress vs. Dislocation Velocity Tests

Specimen No.	Load Pulse Duration	Tensile Stress	Grain No.	Resolved Shear Stress	Dislocation Velocity
	sec	lb/in.^{2}		lb/in.^{2}	cm/sec
T3	1.850	50,100	1	19,700	0.00173
			2	20,050	0.00153
			3	22,850	0.00083
			4	25,000	0.00124
			5	20,850	0.00171
			6	21,800	0.00171
			7	21,200	0.00398
			8	19,600	0.00288
			9	22,400	0.00342
			10	22,150	0.00514
			11	20,800	0.00126
			12	23,400	0.00166
T8	0.529	53,300	1	22,800	0.00586
			2	23,800	0.0158
			3	22,400	0.0132
			4	22,150	0.0151
			5	22,800	0.0173
			6	22,400	0.0155
			7	19,100	0.00567
			8	22,300	0.0195
T2	0.175	55,350	1	23,550	0.0149
			2	24,700	0.0267
			3	24,700	0.0175
T16	0.017	59,400	1	26,000	0.118
			2	26,650	0.113
			3	26,200	0.363
			4	28,600	0.202
			5	25,400	0.177
			6	24,700	0.165
			7	24,800	0.196
			8	27,450	0.333
			9	23,400	0.303
			10	27,400	0.186

TABLE 4-Continued

Specimen No.	Load Pulse Duration	Tensile Stress	Grain No.	Resolved Shear Stress	Dislocation Velocity
	sec	lb/in.^{2}		lb/in.^{2}	cm/sec
T16	0.017	59,400	11	25,050	0.303
			12	28,650	0.461
			13	24,600	0.102
			14	25,550	0.122
			15	25,700	0.130
			16	26,550	0.617
			17	25,200	0.558
			18	27,200	0.647
			19	24,900	0.256
			20	28,650	0.491
			21	24,600	0.141
			22	26,200	0.215
			23	27,000	0.137
			24	26,800	0.166
			25	25,300	0.128

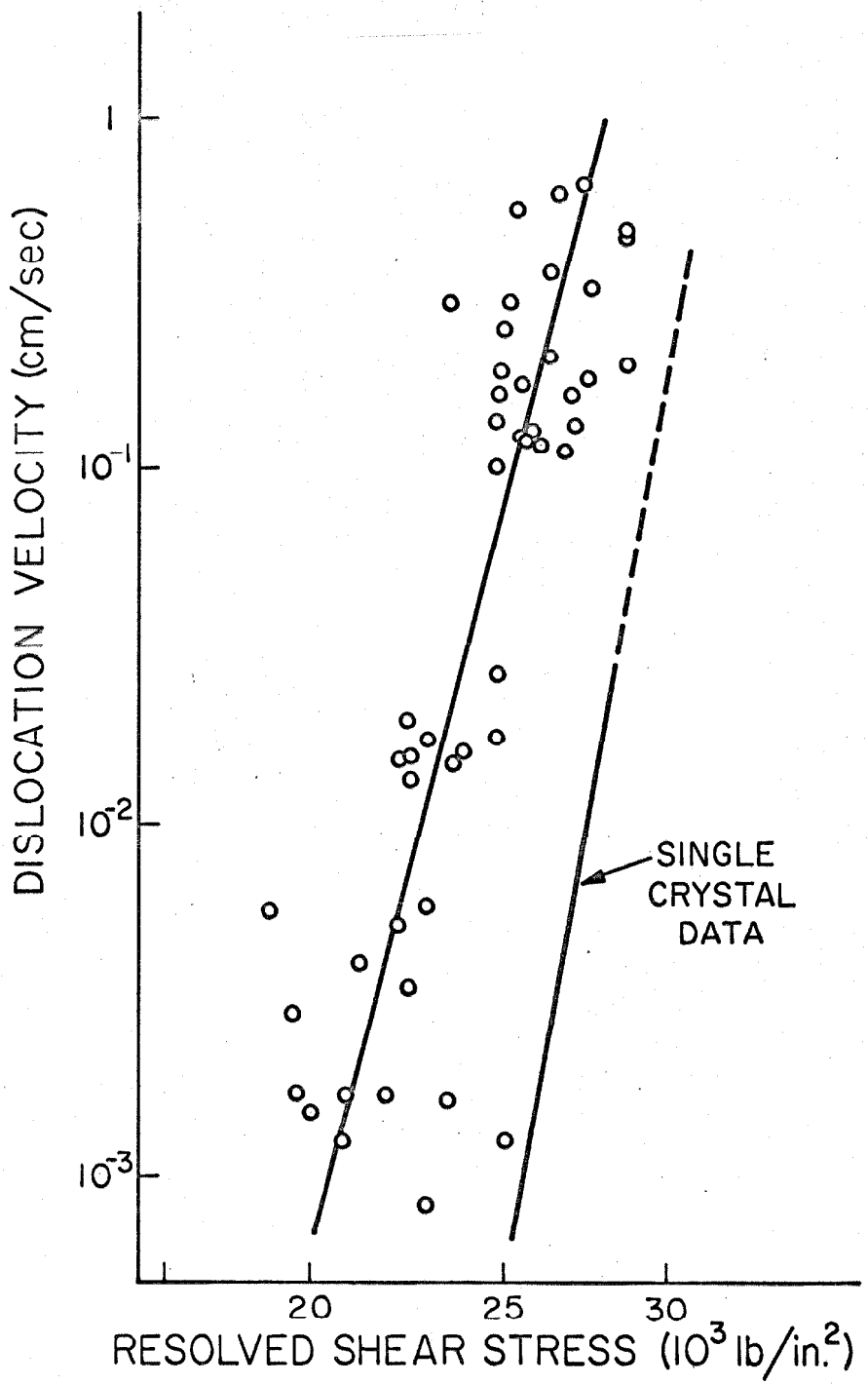

Fig. 24 Stress dependence of dislocation velocity for polycrystalline specimens.

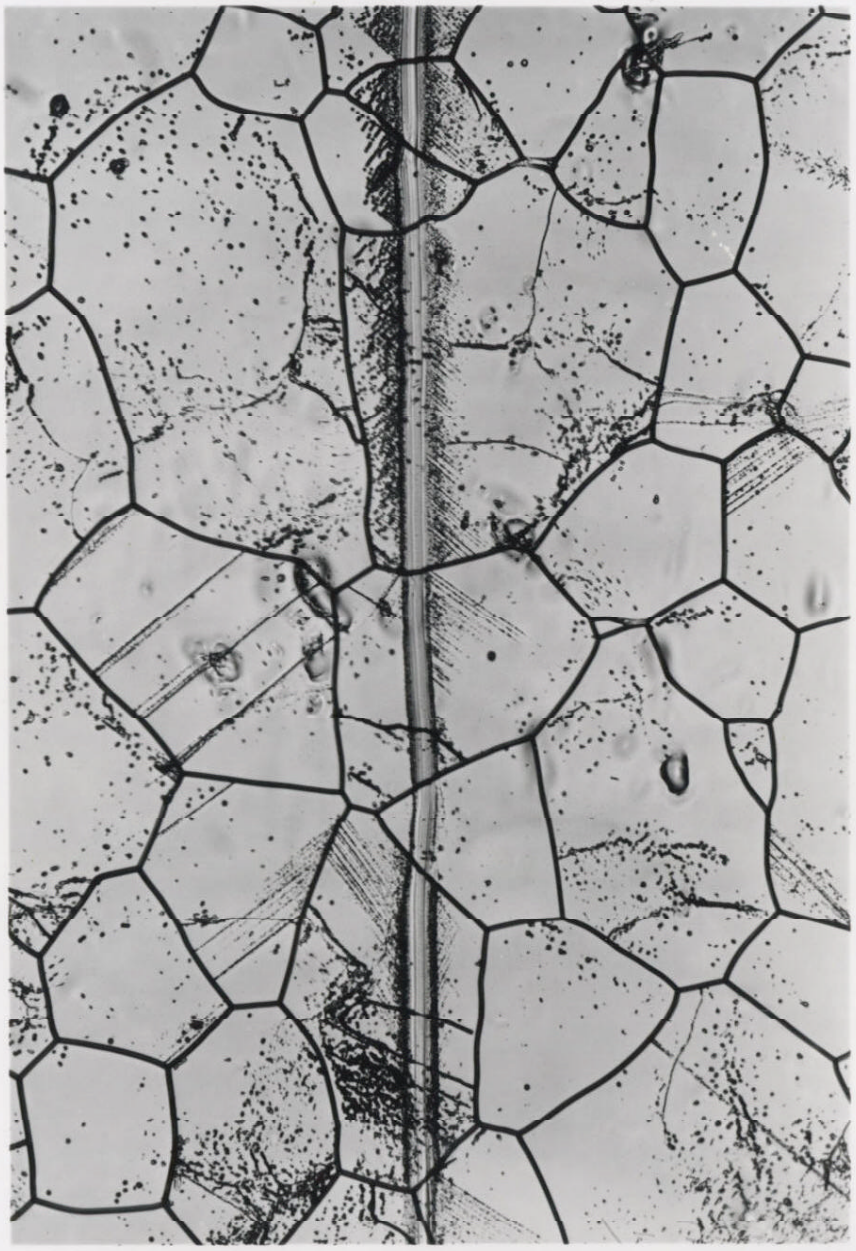

Fig. 25. Typical dislocation configuration in a pulse loaded specimen. Note the dislocation motion in grains that do not contain the fresh scratch. Etched to reveal dislocation sites. Specimen T14. 300X.

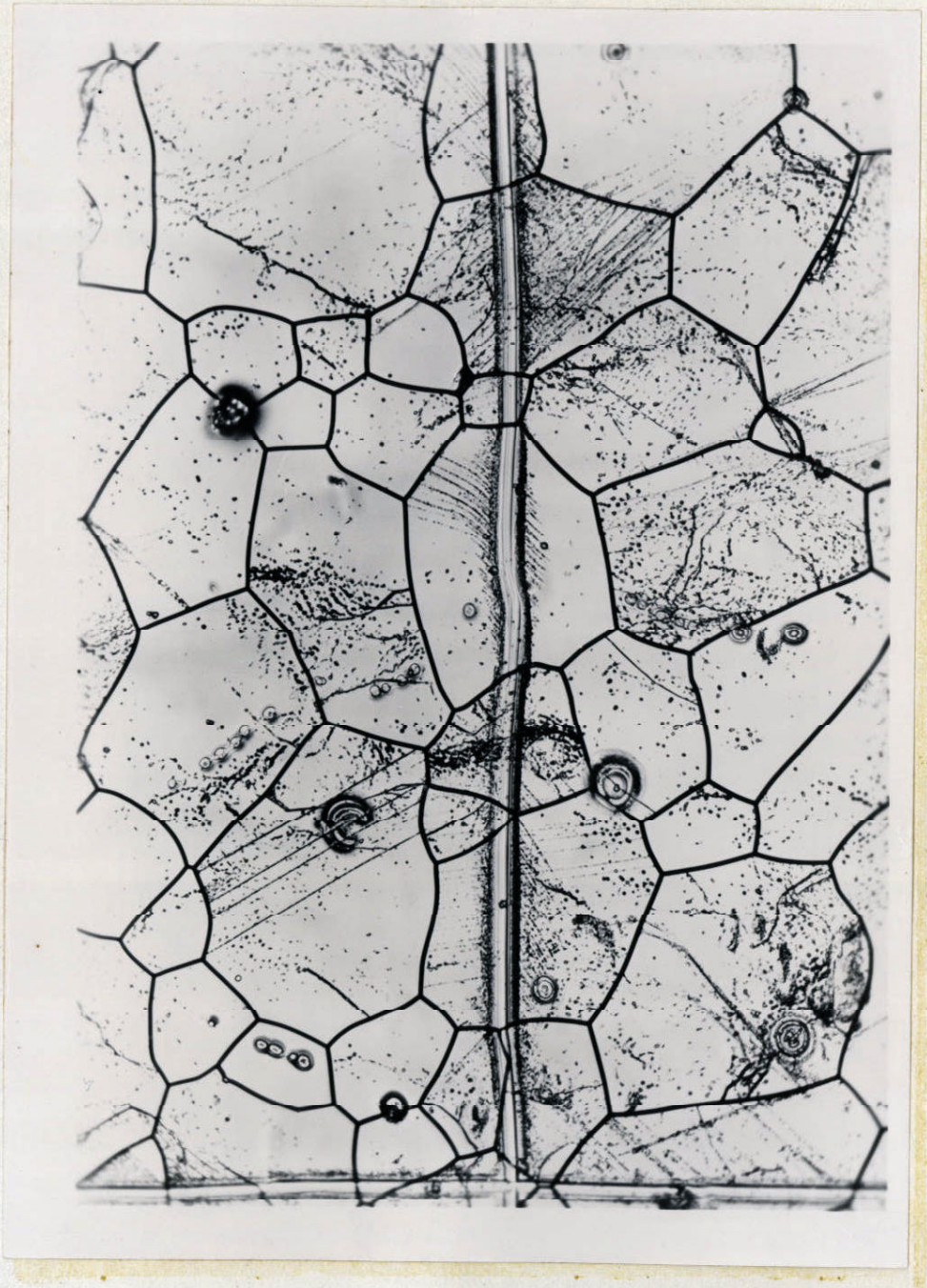

Fig. 26 Photomicrograph of a pulse loaded specimen. Note the dislocation motion away from the fresh scratch. Etched to reveal dislocation sites. Specimen T15. 300X.

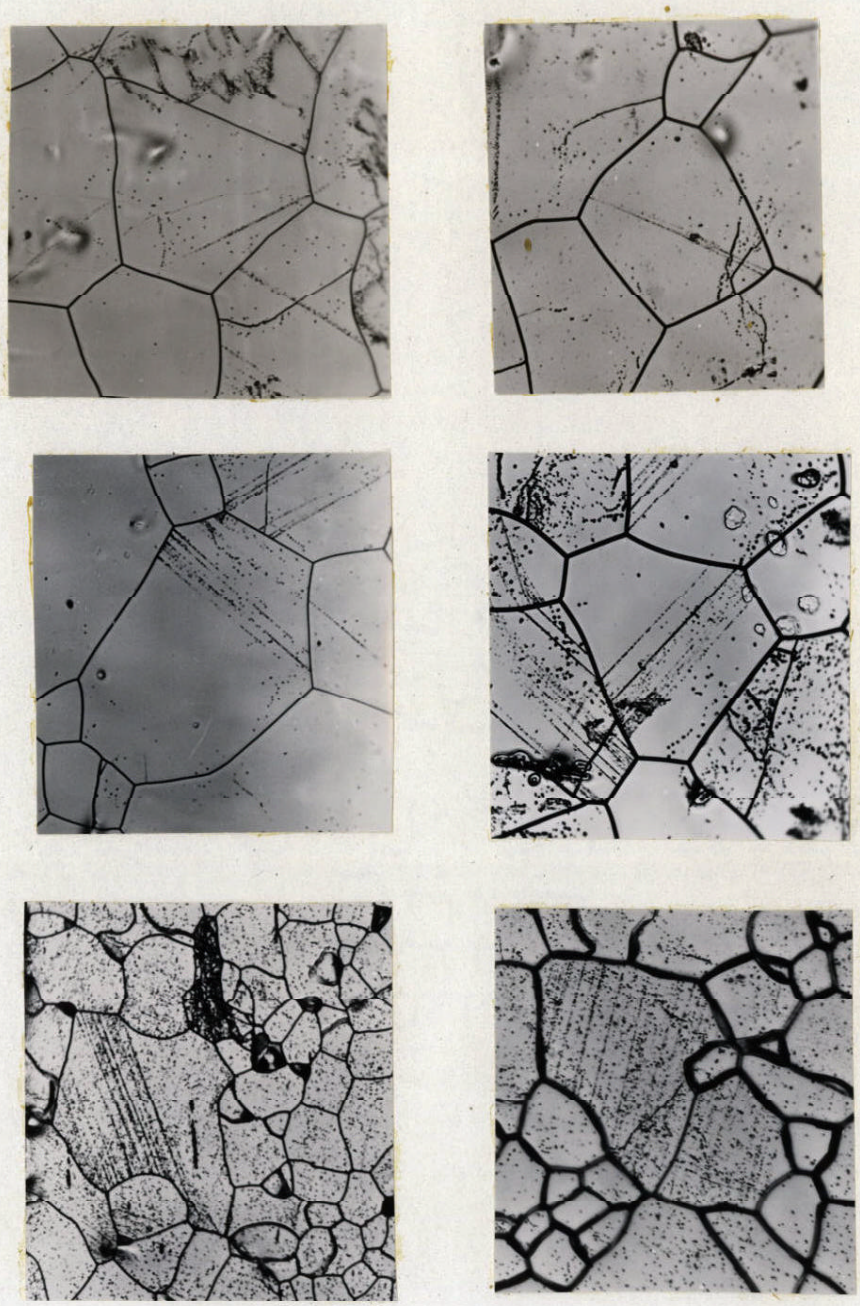

Fig. 27 Photomicrographs of widening slip bands illustrating the mechanics of relaxation. Etched to reveal dislocation sites. 300X.

successive slip lines adjacent to the slip band. The spacing between successive slip lines is approximately constant within the band.

C. Dislocation Velocity Tests in Single Crystals

The results of tests to determine the stress dependence of dislocation velocity in single crystals of silicon-iron are shown in Table 5. The data have been plotted in figure 28. The plot shows that the data may be represented by a relation of the form $v = (\tau/\tau_o)^n$ where $n = 32.6$ and $\tau_o = 31{,}700$ lb/in.^{2}. Column 4 of Table 5 lists the angle between the observed slip trace on the surface of the specimen and the $\langle 111 \rangle$ Burgers vector of the observed active slip system. The observed slip trace is the intersection of the active slip plane and the observation plane (see figure 29).

Slip traces observed on the flat surfaces and exposed edges of the test specimens were used to determine the Miller indices of the slip planes. Due to massive slip in some specimens, it was not possible to identify clearly the slip trace on the exposed edge. All specimens for which two slip traces could be identified clearly yielded on $\{110\}$ planes. For the remaining specimens which revealed only one slip trace which was identified clearly, a further analysis was required.

The $\langle 111 \rangle$ slip direction in BCC iron is well accepted as the only slip direction active during the yielding process (34, 35).

TABLE 5

Results of Single Crystal Tests

Specimen No.	Resolved Stress	Observed Velocity	Angle Between Slip Trace and <111> Direction
	$lb/in.^2$	cm/sec	Degrees
S9	21,300	7.19×10^{-6}	31
S10	22,400	1.02×10^{-5}	27
S9	22,050	1.21×10^{-5}	31
S11	23,200	3.95×10^{-5}	40
S11	24,100	1.46×10^{-4}	40
S11	25,200	3.70×10^{-4}	40
S11	26,800	1.42×10^{-3}	40
S10	26,550	6.01×10^{-3}	27
S12	28,000	2.80×10^{-2}	10

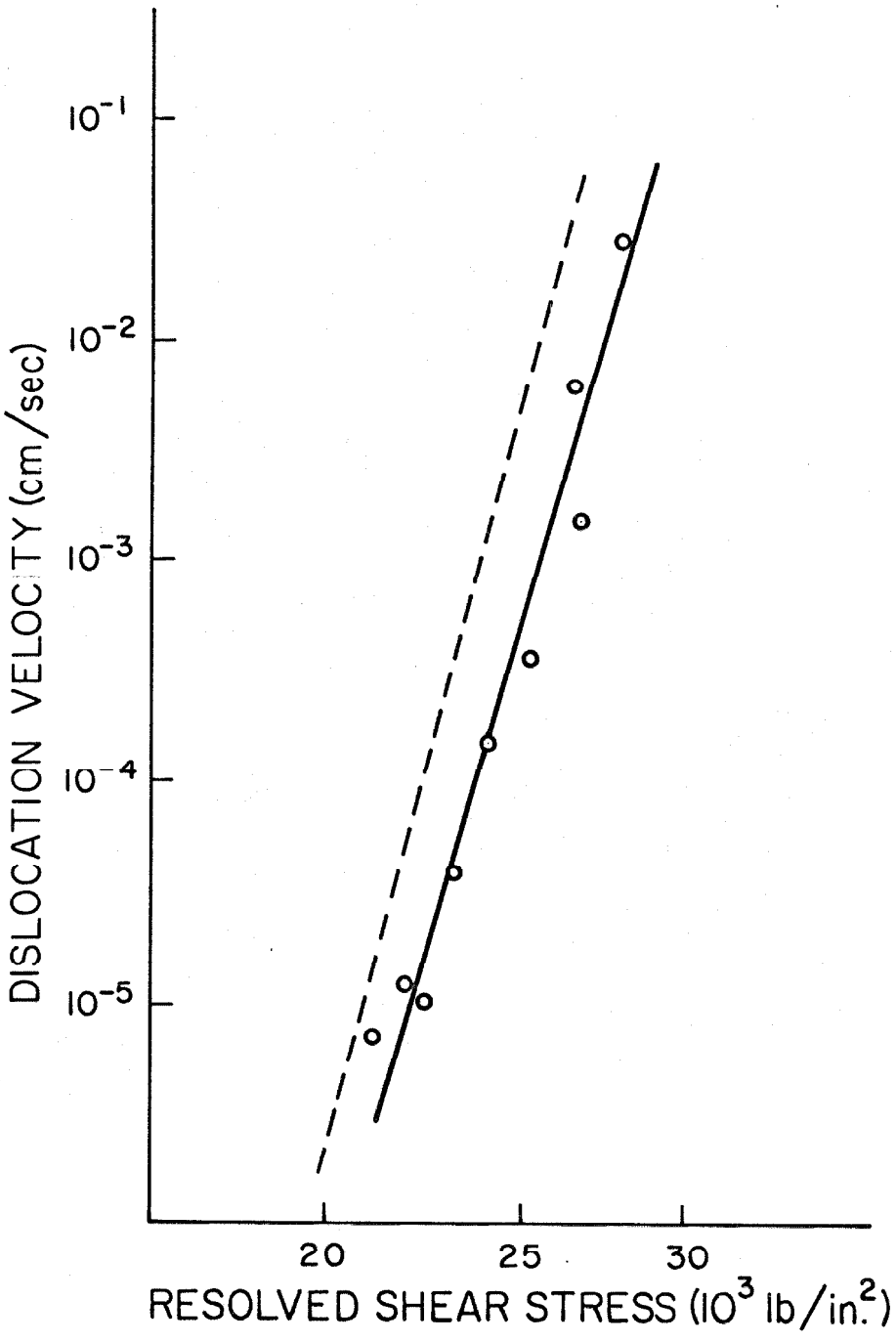

Fig. 28 Stress dependence of dislocation velocity for single crystals. 75°F. Dashed line--Stein and Low data.

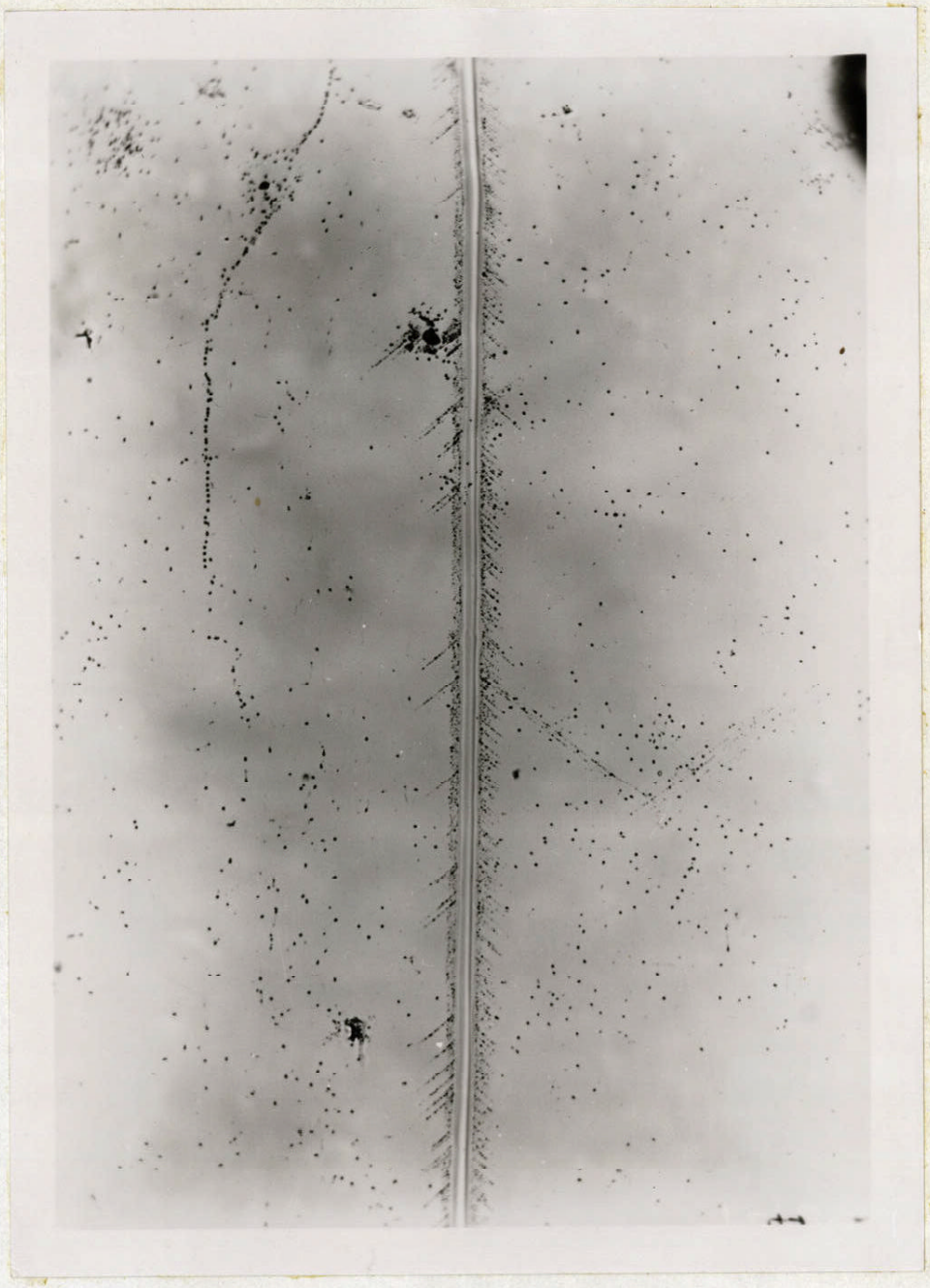

Fig. 29 Typical dislocation configuration after a pulse load in single crystal specimen S9. 300X.

Assuming that $\langle 111 \rangle$ is the slip direction for all single crystals tested, it follows that the maximum number of "possible" slip planes consistent with a single slip trace is four.

The resolved shear stress for each of these "possible" slip systems was calculated. The "possible" slip system subjected to the highest resolved shear stress in all single crystal tests was of the $\{110\}\langle 111 \rangle$ type. Thus it is clear that only $\{110\}$ slip planes were active during the single crystal tests in this investigation.

All attempts to obtain stress vs. dislocation velocity data at higher stress levels than those reported in Table 5 were unsuccessful due to twinning of the test specimens. The twinning stress on the most favorable twin system was calculated for all single crystal specimens by using equation 10. The twin plane for BCC iron is $\{112\}$ and the direction is $\langle 111 \rangle$ (36). Table 6 lists the resolved stress for the most favorable twin systems and the most favorable slip systems. The final mode of deformation observed for each single crystal specimen and the highest stress are also tabulated.

Two of the specimens contained two highly stressed twin systems. The twinning directions for specimen S9 were $[\bar{1}\bar{1}1]$ and $[1\bar{1}1]$, while those for specimen S13 were $[1\bar{1}1]$ and $[11\bar{1}]$. The summation of twinning directions for S9 yields a net $[0\bar{1}1]$ direction while for S13 a $[100]$ direction is obtained. Specimen S13 cleaved along a (100) plane while S9 twinned on two separate planes. Microscopic examination revealed that two separate twin systems were active

TABLE 6

Results of Highest Stress
Applied To Single Crystal Specimens

Specimen No.	Highest Applied Stress $lb/in.^2$	Resolved Stress for Slip {110} ⟨111⟩ $lb/in.^2$	Resolved Stress for Twinning {112} ⟨111⟩ $lb/in.^2$	Final Behavior
S2	61,100	28,400	26,900	Twinning
S3	54,500	25,100	27,200	Twinning
S8	57,300	27,200	28,600	Twinning
S9	56,450	25,200 26,100	28,000 28,200	Twinning
S10	56,450	26,550	26,900	Slip
S11	55,000	26,800	25,500	Slip
S12	56,200	28,000	27,100	Slip
S13	60,000	27,700 26,500	29,400 27,000	Cleavage

adjacent to the cleavage surface of specimen S13. The twin systems observed and their role in nucleating cracks is consistent with previous reports by Hull (34).

The extreme sensitivity of dislocation velocity to small differences in stress provides an excellent method for determining the accuracy of the specimen preparation and loading procedures. The dislocation velocity was determined on both sides of specimen S12 by direct observation, and the difference in stress was calculated on the basis of equation 7.

(a) Front Side Velocity: $v_F = (\tau_F/\tau_o)^n$

(b) Back Side Velocity: $v_B = (\tau_B/\tau_o)^n$

Dividing equation (a) by equation (b):

$$v_F/v_B = (\tau_F/\tau_B)^n$$

or

$$\tau_F/\tau_B = (v_F/v_B)^{1/n}$$

The ratio of observed velocities in specimen S12 was 1.73 which indicates a bending stress equal to 0.85 per cent of the tensile stress.

VI. DISCUSSION OF RESULTS

Source of Dislocations in Polycrystalline Specimens

The observations of slip bands indicate that in fully annealed material the grain boundary was the initial source for slip band growth. The distribution of individual etch figures within the slip bands which do not traverse the entire grain shows a decreasing density of dislocations with increasing distance from the grain boundary. Slip band growth by the cross-slip mechanism proposed by Koehler (21) should produce slip bands with dislocation densities which decrease as the distance from the source increases. This is seen in the slip bands in polycrystalline silicon-iron emanating from fresh scratches which show a dislocation density decreasing with distance from the scratch when the slip band does not reach a grain boundary. All slip bands appearing in fully annealed polycrystalline specimens (without scratches) are observed to have at least one end originating in a grain boundary. If the primary sources of dislocations were uniformly distributed throughout the matrix, then at least some evidence should be obtained in which both ends of a slip band terminate within a grain. This would especially be true for specimens subjected to short duration pulse loading. However, the grain boundaries are the primary sources. This is in agreement with Worthington and Smith (37). They reported that slip bands are nucleated at grain boundaries in 3 per cent silicon-iron statically loaded to produce pre-yield microstrain.

The observations of slip band growth in polycrystalline specimens indicate that an initial stress is required to initiate the slip bands at the grain boundaries. The relative ease with which fresh dislocations move in a scratched grain is clearly shown in figures 24 and 25. The number of slip lines formed from the fresh scratch is much greater than the number formed from the grain boundaries. Furthermore, a high percentage of the scratched grains developed slip lines in the stress pulse tests. Only a very low percentage of the unscratched grains shows any slip lines. These observations indicate that a critical resolved stress greater than the friction stress is required to initiate slip in a fully annealed grain, and that grains which do not show slip at a given σ , could form slip bands when sources are introduced or when σ is increased. This conclusion that a critical stress greater than the friction stress is required to initiate slip in fully annealed material will be used in the delay-time model to be presented below.

Stress--Dislocation Velocity Relations

A. Single Crystal Specimens

The velocity of mobile dislocations in single crystals of silicon-iron was found to be a very sensitive function of the applied stress. Figure 28 shows that the empirical equation $v = (\tau/\tau_0)^n$ used by Stein and Low could also be used to fit the data obtained here with small differences in τ_0 and n .

Two factors which are probably responsible for these differences are the initial total dislocation density and the crystal orientation.

An increase in the dislocation density would be expected to raise τ_o because of the increased number of dislocation interactions. The effect of dislocation density on n in silicon-iron is unknown. Stein and Low observed displacement of edge dislocations in crystals having 10^5 dislocations/cm^2 prior to scratching, while in this investigation the displacements of dislocations of mixed edge and screw components were observed in crystals having an initial density of 10^{+6} to 10^{+7} dislocations/cm^2. The higher value of τ_o obtained here is consistent with the greater initial density.

Low and Guard (19) have shown that dislocation loops in silicon-iron are very much elongated in the direction of the Burgers vector. This indicates that the velocity of screw oriented dislocations is much less than the velocity of edge oriented dislocations with the same applied stress. The slip bands observed in this investigation had Burgers vectors which intersected the slip traces at angles large enough to preclude the observation of the maximum dimension of the slip band which is established by the velocity of edge oriented dislocations. Such elongation of the dislocation loops would make the present observation of dislocation displacements the result of essentially screw oriented dislocation motion. The difference between the τ_o obtained from the present data for screw dislocations in slip bands and the τ_o obtained for edge oriented dislocations by Stein and Low is consistent with the observations of the slip band shape, i.e., slip bands grow faster in the direction of the Burgers vector.

The data obtained could also satisfy an expression of the form $v = v_c e^{-D/\tau}$ for the range of velocities observed (11). The values $v_c = 10^{10}$ cm/sec and $D = 768{,}000$ lb/in.^{2} were obtained from a plot of the data. The value of v_c (the limiting velocity at infinite stress) should be the shear wave velocity of the material, approximately 10^5 cm/sec in silicon-iron. The value of $v_c = 10^{10}$ cm/sec is too high for any physically meaningful interpretation of the data based on the expression $v = v_c e^{-D/\tau}$.

A more critical determination of the functional relation between dislocation velocity and stress can be made by extending the range of direct observation data beyond that presently available. All attempts to obtain data at stress and velocity levels above those shown in figure 25 failed because of twinning in the tensile specimens. The resolved twinning stress for 3 per cent silicon-iron single crystals is between 26,900 lb/in.^{2} and 28,200 lb/in.^{2} in rapidly applied tensile tests at 75°F. Stein and Low obtained their stress vs. dislocation velocity data in 3-point bending tests of single crystals and did not report the occurrence of twinning in their specimens at room temperature. The maximum velocity observed by Stein and Low was 10^{-2} cm/sec and was limited by the method of loading. The maximum velocity observed in this investigation was 2.8×10^{-2} cm/sec, while the maximum velocity capability of the experimental equipment was at least 25 cm/sec with the specimens described earlier. The specimens used by Stein and Low were oriented so that only single slip occurred. The angle from the tensile stress

axis to the slip plane $\{110\}$ was 45 degrees and the angle to the slip direction $\langle 111 \rangle$ was 45 degrees. This orientation caused the observed slip system to be subjected to the highest resolved shear stress of any possible slip or twinning system in the crystal.

B. Polycrystalline Specimens

The experimental measurements of the velocity of fresh dislocations in single crystals show relatively little deviation from a linear relationship between log τ and log v. A relatively large deviation from a linear relationship between log τ and log v is found in the polycrystalline data. The initial density of dislocations and the chemical composition of both single crystal and polycrystalline specimens were nearly equal. Testing temperature and loading rate were also equal or equivalent for both types of tests. Therefore, the "scatter" of the polycrystalline results must be due to deviations in the resolved shear stress on the slip systems from that calculated from the tensile stress and the Schmid factor. The deviations are attributed to the effect of elastic anisotropy on the actual stress distribution in the polycrystalline specimens. A maximum deviation of 25 per cent in stress is observed between the results obtained with the single crystal and polycrystalline specimens. This deviation is reasonable in view of the variation in elastic properties with crystal orientation (38).

All points based upon the tests with polycrystalline specimens lie above the curve for data on single crystal specimens, see figure

24. This is because the duration of the stress pulse used to determine τ vs. v in polycrystalline specimens was such that data was obtained only in the highly stressed grains. A short duration pulse test at a constant σ produces data from only those grains containing the highest resolved shear stress. Longer duration pulses will allow the slip band to traverse the most highly stressed grains. The pulse duration was chosen so that very few grains were completely traversed. Data was therefore obtained from only the most highly stressed grains.

Delay-Time for Yielding in Fine Grain Polycrystalline Specimens

The delay-time phenomenon is an intriguing aspect of the plastic deformation behavior of BCC metals containing interstitial impurities. The discovery of a delay-time for yielding in low-carbon steel by Clark and Wood has provoked a large number of investigators to ponder the cause or causes and the mechanics of the deformation processes that occur during the transition from elastic deformation to a fully developed, macroscopic plastic deformation.

The sequence of events leading to the formation of a Luder's band has been observed in this investigation by the use of the pulse loading and electrolytic etching techniques. These observations, together with the observations of the stress dependence of dislocation velocity will be used to develop a semi-quantitative description of the dislocation mechanics leading to the formation of the Luder's band.

The following explanation of the yielding of silicon-iron is based on three assumptions: first, that dislocation sources are

not activated until a critical resolved shear stress τ_c is reached which is greater than the friction stress τ_f; second, that the rate of yielding is governed by the dislocation velocity which is a sensitive function of stress and varies considerably from grain to grain; and third, that the delay-time is essentially given by the time for the yielded region to spread continuously through the thickness at some section of the specimen. This section is called the critical section.

The strain vs. time relation for fine grain polycrystalline silicon-iron subjected to a constant stress can be explained as follows. The initial high plastic strain rate is the result of the rapid relaxation of the highest resolved shear stresses in certain grains and to a small degree from grains with lower resolved shear stresses. The variation in resolved shear stress from grain to grain is the result of two factors: a) the grains are oriented differently and hence have different Schmid factors, and b) the elastic moduli of neighboring grains differ when referred to common axes because of elastic anisotropy. The strain rate decreases as the highly stressed grains are relaxed. The fraction of the total grains relaxed at any time will be dependent on the applied stress. Applied stresses less than σ_{uy} and great enough to produce τ_c in some grains produce a strain rate that decreases to zero. The structure at this point shows essentially isolated relaxed grains because stresses on adjacent grains are insufficient to generate slip bands. As the stress is increased, more grains relax and clusters of relaxed grains appear. An applied stress equal to the

upper yield point stress will result in a zero strain rate. However, the duration of this condition is indeterminate. The effect of the relaxation of those grains which have yielded prior to general yielding is to increase the resolved shear stress on less favorably oriented grains to a value which will initiate slip bands in the adjacent grains. The clusters of relaxed grains cause a local stress concentration on adjacent grains (proportional to the square root of the cluster diameter). When the upper yield stress is reached, the stress concentration is sufficient to cause one of the clusters of yielded grains to extend through the thickness of the specimen.

At this stage, the stress concentration factor increases significantly and the band rapidly spreads to cover a cross-section of the specimen. This results in a relatively sudden increase in the strain rate which marks the end of the delay period. When a cross-section of the specimen is completely covered by relaxed grains the Luder's band is distinguishable by its characteristic surface deformation and propagates as a stable front along the length of the specimen. The propagation velocity of the Luder's band is less than the growth rate of the embryonic band across a cross-section because the value of the stress concentration factor decreases when the elastic-plastic transition region extends across the entire specimen. The time for yielding to occur under constant applied stress is then essentially the time for an embryonic Luder's band to grow across the thickness of a specimen.

The delay-time in fine grain silicon-iron observed in this investigation ranged from 0.010 to 0.263 sec for applied constant stresses between 71,500 and 74,600 lb/in.^{2}. Assuming an applied stress of 72,400 lb/in.^{2} and an ideally oriented grain ($\phi = 45°$, $\lambda = 45°$) within a polycrystalline matrix, the nominal resolved shear stress on the grain would be 36,200 lb/in.^{2}. The velocity of a dislocation in this grain obtained by extrapolating the curve in figure 28 would be approximately 340 cm/sec. At this velocity the dislocation would cross the ideally oriented grain in about 7.5×10^{-6} sec. The delay-time for yielding is at least 10^3 to 10^4 greater than the time necessary for individual dislocations to traverse the ideally oriented grains in a specimen.

The complete relaxation of a grain does not occur with the formation of the first slip band. A family of slip bands is observed to build up by the addition of one new slip band at a time adjacent to an existing slip band at a characteristic distance h. The characteristic spacing, h, must be a function of the stress and test temperature, but does not appear to be a very sensitive function of stress. A value of $h = 0.91 \times 10^{-4}$ in. has been reported for statically loaded silicon-iron by Hibbard and Dunn (39). Average values for h in randomly oriented grains in this investigation were 0.95×10^{-4} in. for static tests and 0.96×10^{-4} in. for pulse tests. Stress concentrations at grain boundaries near the end of a slip line tend to reduce h by activating dislocations on parallel slip systems

close to the existing slip band. Interaction of dislocations on the old slip band and on the newly forming slip band tends to increase h.

The delay-time required to relax a grain by the above model, one slip line at a time, would be d/h times the traverse time necessary for the formation of one slip band across the grain. The average relaxation time for an ideally oriented grain in the fine grain material at an applied stress of 72,400 lb/in.^{2} would be ten times the traverse time for a single slip line, or about 7.5×10^{-5} sec, if the stress in the grain is assumed to be constant. This relaxation time is still 10^2 to 10^3 less than the observed delay-time. However, all grains are not ideally oriented and the time to relax less favorably oriented grains is significantly longer. The fine grain specimens contained approximately ten grains through their thickness, and the delay-time for yielding can be calculated from the dislocation velocity vs. stress data if the stress is estimated for each grain at the critical cross-section. Such an estimation is very difficult. In view of the very high sensitivity of dislocation velocity to stress, the delay-time will essentially be governed by the time to relax the grain that has the lowest stress (i.e., lowest Schmid factor). Therefore, the delay-time will be approximately given by

$$t_D = \frac{d^2}{h V_{min}} \qquad (12)$$

where d is the diameter of the grain in the critical section having the lowest resolved shear stress, h is the spacing between adjacent

slip bands in the grain and V_{min} is the dislocation velocity in the grain.

The minimum velocity V_{min} is given by

$$V_{min} = \left(\tau_{min} / \tau_o \right)^n \qquad (13)$$

but again τ_{min} cannot be accurately estimated. The expression

$$\tau_{min} = m S \sigma \qquad (14)$$

where

m = stress concentration factor due to surrounding relaxed grains and anisotropy,

S = Schmid factor and

σ = nominal applied tensile stress,

will be used to calculate a value for τ_{min} based on the observed values of t_o , h , $\bar{d}$, n and τ_o obtained in this investigation. Combining the above expressions gives the delay-time as

$$t_D = \left(\frac{\tau_o}{m S} \right)^n \frac{\bar{d}^2}{h} \sigma^{-n} \qquad (15)$$

Consider a typical delay-time test shown in Table 3. For specimen M21, t_D = 0.036 sec, h = 10^{-4} in., $\bar{d}$ = 10^{-3} in., n = 32.6 and τ_o = 31,700 when the nominal stress was 73,300 lb/in.^{2}. From equation 12,

$$V_{min} = \frac{\bar{d}^2}{h\, t_D} = \frac{10^{-6}}{3.6 \times 10^{-4} \times 10^{-2}}$$

$$V_{min} = \frac{1}{3.6} \text{ cm/sec}$$

and from equation 13,

$$\tau_{min} = \tau_o (V_{min})^{1/n} = (31{,}700)\left(\frac{1}{3.6}\right)^{\frac{1}{32.6}}$$

$$\tau_{min} = 30{,}800 \text{ lb/in.}^2$$

which, when substituted into equation 14, gives

$$mS = \tau_{min}/\sigma = 30{,}800/73{,}300$$

$$mS = 0.420$$

The value of 0.420 is reasonable for the product of stress concentration factor and Schmid factor for a poorly oriented grain, in view of the fact that S can be as low as 0.278.

The stress dependence of the delay-time is the same as the stress dependence of the dislocation velocity. The temperature dependence of the delay-time results from the temperature dependence of the dislocation velocity as postulated by Hahn (4) and Cottrell (24).

The foregoing discussion has explained the appearance of a true upper yield point, the observed plastic strain vs. time behavior at constant stress and the delay-time for yielding at constant stress in silicon-iron.

Luder's Band Propagation and Average Dislocation Velocity

It is well known (37, 38) that steady-state propagation of a Luder's band occurs at constant stress. The band front or transition region between plastically deformed material and relatively virgin material must contain a wide range of strains in relative equilibrium with a constant applied stress. The leading edge of a propagating Luder's band contains dislocations moving into unstrained material. Behind the leading edge dislocation interactions with grain

boundaries, other dislocations and impurities lead to reduced velocity of the dislocations until at some macroscopic value of strain, the stress induced dislocation configuration reaches a static equilibrium with the applied stress. This value of strain is called the Luder's strain.

The propagating Luder's band is composed of grains in which slip bands are forming. The stress dependence of the velocity of propagation of the Luder's band must be related to the stress dependence of individual dislocation velocities. Consider the steady-state strain configuration of a Luder's band front as it propagates along a uniaxial tension specimen. Hart (40) has shown that the strain rate at any point on the propagating front must be

$$\dot{\epsilon} = V_B \left(d\epsilon / d\ell \right) \tag{16}$$

where

V_B = propagation velocity of the band front,

ϵ = natural strain and

ℓ = length along the specimen measured on a coordinate system moving with .

Note that for small strains, the natural strain is approximately equal to the engineering strain. The length ℓ is related to the specimen by $\ell = x - V_B t$ where x is the distance along the specimen. Assuming that the strain distribution within the moving Luder's band front remains constant and propagates along the specimen at V_B, then the strain ϵ is given by

$$\epsilon = f(\ell) \tag{17}$$

The total change in length, e, of the specimen at any time is given by

$$e = \int_0^L \epsilon \, dx = \int_0^L f(\ell) \, dx \tag{18}$$

and the rate of change of the length of the specimen, crosshead speed, is

$$\frac{de}{dt} = \int_0^L \frac{df}{dt} \, dx \tag{19}$$

From equations 16 and 17 it follows that

$$\frac{df}{dt} = V_B \left(\frac{d\epsilon}{d\ell} \right) \tag{20}$$

and the rate of specimen extension de/dt becomes

$$\frac{de}{dt} = \int_0^L V_B \left(\frac{d\epsilon}{d\ell} \right) dx \tag{21}$$

If the propagation velocity is constant, then at any given time

$$\frac{de}{dt} = V_B \, \epsilon \Big|_{x=0}^{x=L} = V_B \left[f(x - V_B t) - f(-V_B t) \right] \tag{22}$$

The points $x = 0$ and $x = L$ are the ends of the specimen. As long as the Luder's band front is between these extremes and only one front is moving,

$$f(L - V_B t) - f(-V_B t) = \epsilon_L \tag{23}$$

where ϵ_L is the total strain produced by the moving front.

Thus the rate of extension, de/dt, is related to the propagation velocity, V_B, and the Luder's strain, ϵ_L, by

$$\frac{de}{dt} = V_B \epsilon_L \tag{24}$$

Measurement of de/dt and ϵ_L can therefore be used to determine the propagation velocity. The propagation of a Luder's band in silicon-iron occurs at constant stress as shown in figure 18. Therefore, the velocity of the crosshead is equal to the extension rate of the specimen, $V_{cs} = de/dt$, and the Luder's band velocity is

$$V_B = V_{cs}/\epsilon_L \tag{25}$$

for a single moving front.

The total elongation rate of a single specimen is the sum of the contributions from each moving front in a specimen containing multiple moving Luder's band fronts, n. The velocity of each moving front may not be constant and hence equation 21 may be difficult to evaluate. For the special case of $n = 2$, in which both moving fronts traverse equal lengths of the specimen in equal times, the average velocity of each must be the same. Treating V_B in equation 21 as the average velocity for each moving front then leads to

$$V_B = V_{cs}/2\epsilon_L \tag{26}$$

which was used to derive the data shown in Table 2.

The strain rate of any material was given by equation 3 as $\dot{\gamma} = b\rho_m v$, from which it follows that

$$\dot{\epsilon} = \rho_m K v \tag{27}$$

where K is a constant which depends on the Burgers vector of the dislocations and the orientation of the operative slip system with respect to the specimen axis, ρ_m is the density of moving dislocations and v is the average velocity of moving dislocations. Equating 16 and 27 results in

$$V_B = K\rho_m v \Big/ \frac{d\epsilon}{dl} \tag{28}$$

The strain distribution $\epsilon(l)$, density of moving dislocations ρ_m and average dislocation velocity v have been shown to be functions of the applied stress. However, the velocity v is much more sensitive to stress than is $\epsilon(l)$. For a first order approximation, $d\epsilon/dl$ may be assumed to be constant. Then equation 28 becomes

$$V_B = K'\rho_m v \tag{29}$$

which combined with equation 7 yields

$$V_B = K''\rho_m \sigma^n \tag{30}$$

Taking logarithms of both sides of equation 30 and differentiating with respect to log σ ,

$$\frac{\partial \log V_B}{\partial \log \sigma} = \frac{\partial \log \rho_m v}{\partial \log \sigma} \equiv m = \frac{\partial \log \rho_m}{\partial \log \sigma} + n \quad (31)$$

in which n is the usual mobility exponent.

The above development will now be compared with the experimental results by obtaining the stress dependence of the observed velocity of the Luder's band front. Consider the slope of the curve shown in figure 19. The $\log_{10}(10 \times V_B)$ goes from 0 to 2.5 when stress changes from 62,100 to 67,000 lb/in.^{2}, and

$$\log_{10}(10 \times V_B) = \frac{2.5}{5500}(\sigma - 62,100) \quad (32)$$

Note that $\frac{1}{2.3}\log_{10}\chi = \log_e \chi \approx \chi - 1$, $\chi < 1$ and the right side of equation 32 may be written

$$\frac{2.5}{5500}(62,100)\left(\frac{\sigma}{62,100} - 1\right) = 65 \log_{10}\left(\frac{\sigma}{62,100}\right) \quad (33)$$

and

$$\log_{10}(10 \times V_B) = 65 \log_{10}\left(\frac{\sigma}{62,100}\right) \quad (34)$$

or finally

$$V_B = 0.1\left(\frac{\sigma}{62,100}\right)^{65} \quad (35)$$

where V_B is in in./min. and σ is in lb/in.^{2}. The logarithmic derivative of equation 35 with respect to $\log \sigma$ is

$$m = \frac{\partial \log V_B}{\partial \log \sigma} = 65 \quad (36)$$

The value of $m = 65$ determined experimentally by Luder's band propagation is approximately twice as large as the value of $n = 32.6$, determined by the direct observation of dislocation motion in single crystal specimens. Guard (41) has experimentally determined the value of m in equation 31 by measurements of the strain rate sensitivity. He obtained values of m between 62 and 70 in 3 per cent silicon-iron. Noble and Hull (42) have more recently reported values of m between 75 and 89 at low strain in polycrystalline silicon-iron deduced from measurements of stress relaxation at constant total strain.

The experimental results obtained here are in good agreement with the results obtained by Guard and by Noble and Hull. Luder's band propagation velocity appears to be equally sensitive to the stress dependence of mobile dislocation density and to the stress dependence of dislocation velocity. The stress dependence of the mobile dislocation density in a propagating Luder's band front can be determined from equation 31 and the observed values of and

From equation 31,

$$\frac{\partial \log \rho_m}{\partial \log \sigma} = 32.4 \qquad (37)$$

from which it follows that

$$\rho_m \approx \sigma^{32.4} . \qquad (38)$$

VII. SUMMARY AND CONCLUSIONS

There were two objectives of this experimental investigation. One was to obtain new data on the microdynamics of dislocations and the dislocation configurations during the transition from the upper yield stress to the lower yield stress. The second was to examine the current theories in order to obtain a better understanding of the macroscopic behavior of BCC materials containing interstitial impurities.

An experimental program was conducted in which the etch pit technique was used for the direct observation of dislocation configurations. Single crystal and polycrystalline tensile specimens of 3 per cent silicon-iron were loaded by the use of an Instron testing machine and a Rapid Load Testing Machine.

The following summary of results and conclusions applies specifically to the broad category of BCC materials containing interstitial impurities.

1. Grain boundaries are the primary source of dislocations for slip band formation in materials containing strongly pinned dislocations.

2. The critical resolved shear stress for grain boundary dislocation source activity is greater than that necessary to propagate fresh dislocations. The difference between the resolved stress for source activity and the resolved stress for propagation makes possible a true static upper yield point in polycrystalline materials which is consistent with models of the upper yield point based on dislocation kinetics.

3. The stress dependence of screw dislocation velocities in single crystals can be fitted to $v = (\tau/\tau_o)^n$ with $n = 32.6$ and $\tau_o = 31{,}700$ lb/in.^{2}. The results obtained here are in good agreement with those of Stein and Low (9). The small differences between the results here and those of Stein and Low are attributed to the intial dislocation density and crystal orientation with respect to the observation surface.

4. Direct observations were made of dislocation mobility in polycrystalline specimens. The scatter in the plotted data of dislocation velocity vs. nominal resolved shear stress is due to anisotropy. All data were obtained from highly stressed grains. The local stress concentration factor resulting from anisotropy was 1.25, based upon the nominal resolved shear stress.

5. A new model of the delay-time for yielding at constant applied stress is presented. Three assumptions are a) no dislocation motion occurs below a critical resolved shear stress, b) the yielding rate is dependent upon the velocity of mobile dislocations and the end of the delay period occurs when yielding of the grains has spread continuously through the thickness of the specimen. This model is consistent with the experimental observations and explains: a) the true static upper yield point, b) the shape of the strain vs. time curve at constant applied stress. The model also yields reasonable values for the stress concentration factor on grains in the critical cross-section that are least favorably oriented for slip.

3. The stress dependence of screw dislocation velocities in single crystals can be fitted to $V = (\tau/\tau_0)^n$ with $n = 32.6$ and $\tau_0 = 31{,}7000$ lb/in.^{2}. The results obtained here are in good agreement with those of Stein and Low (9). The small differences between the results here and those of Stein and Low are attributed to the initial dislocation density and crystal orientation with respect to the observation surface.

4. Direct observations were made of dislocation mobility in polycrystalline specimens. The scatter in the plotted data of dislocation velocity vs. nominal resolved shear stress is due to anisotropy. All data were obtained from highly stressed grains. The local stress concentration factor resulting from anisotropy was 1.25, based upon the nominal resolved shear stress.

5. A new model of the delay-time for yielding at constant applied stress is presented. Three assumptions are a) no dislocation motion occurs below a critical resolved shear stress, b) the yielding rate is dependent upon the velocity of mobile dislocations and c) the delay-time is terminated when yielding of the grains has spread continuously through the thickness of the specimen. This model is consistent with the experimental observations and explains: a) the true static upper yield point, b) the shape of the strain vs. time curve at constant applied stress. The model also yields reasonable values for the stress concentration factor on grains in the critical cross-section that are least favorably oriented for slip.

6) Luder's band propagation velocity appears to be equally sensitive to the stress dependence of dislocation density and velocity.

REFERENCES

1. P. B. Hirsch, A. Howie and M. J. Whelan, "A Kinematical Theory of Diffraction Contrast of Electron Transmission Microscope Images of Dislocations and Other Defects," Philosophical Transactions (1960), Vol. 252, pp. 499-529.

2. J. C. Suits and B. Chalmers, "Plastic Microstrain in Silicon-Iron," Acta Metallurgica (1961), Vol. 9, pp. 854-860.

3. T. Vreeland, Jr., D. S. Wood and D. S. Clark, "Pre-yield Plastic and Anelastic Microstrain in Low-Carbon Steel," Acta Metallurgica (1953), Vol. 1, pp. 414-421.

4. G. T. Hahn, "A Model for Yielding with Special Reference to the Yield-Point Phenomena of Iron and Related BCC Metals," Acta Metallurgica (1962), Vol. 10, pp. 727-738.

5. D. W. Moon and T. Vreeland, Jr., Final Technical Report, National Science Foundation G8187, California Institute of Technology, 1964.

6. C. G. Dunn and F. W. Daniels, "Formation and Behavior of Subboundaries in Silicon-Iron Crystals," Transactions, American Institute of Mining (Metall.) Engineers (1951), Vol. 191, pp. 147-154.

7. T. L. Russell, D. S. Wood and D. S. Clark, Fifth Interim Technical Report under Office of Ordnance Research, Contract No. DA-04-495-ORD-171, California Institute of Technology, 1958.

8. N. J. Petch, "The Cleavage Strength of Polycrystals," Journal of the Iron and Steel Institute (1953), Vol. 174, pp. 25-28.

9. D. F. Stein and J. R. Low, Jr., "Mobility of Edge Dislocations in Silicon-Iron Crystals," Journal of Applied Physics (1960), Vol. 31, pp. 362-369.

10. G. Schoeck, "Correlations Between Dislocation Length and Velocity," Journal of Applied Physics (1962), Vol. 33, p. 1745.

11. W. G. Johnston and J. J. Gilman, "Dislocation Velocities, Dislocation Densities and Plastic Flow in Lithium Fluoride Crystals," Journal of Applied Physics (1959), Vol. 30, pp. 129-144.

REFERENCES--Continued

12. A. H. Cottrell, "The Yield Point in Single Crystal and Polycrystalline Metals," Symposium on the Plastic Deformation of Crystalline Solids, Mellon Institute (1950), pp. 60-73.

13. D. S. Clark and D. S. Wood, "The Time Delay for the Initiation of Plastic Deformation at Rapidly Applied Constant Stress," Proceedings of the American Society for Testing Materials (1949), Vol. 49, pp. 717-735.

14. A. H. Cottrell, Dislocations and Plastic Flow in Crystals (1953), Oxford University Press, London, p. 141.

15. Ibid., pp. 146-147.

16. J. C. Fisher, "Application of Cottrell's Theory of Yielding to Delayed Yield in Steel," Transactions, American Society for Metals (1955), Vol. 47, pp. 451-462.

17. A. H. Cottrell, "Deformation of Solids at High Rates of Strain," Report of a Conference on the Properties of Materials at High Rates of Strain (1957), Institution of Mechanical Engineers.

18. T. L. Russell, D. S. Wood and D. S. Clark, "The Influence of Grain Size on the Yield Phenomenon in Steel," Acta Metallurgica (1961), Vol. 9, pp. 1054-1063.

19. J. R. Low, Jr. and R. W. Guard, "The Dislocation Structure of Slip Bands in Iron," Acta Metallurgica (1959), Vol. 7, pp. 171-179.

20. J. R. Low, Jr. and A. M. Turkalo, "Slip Band Structure and Dislocation Multiplication in Silicon-Iron Crystals," Acta Metallurgica (1962), Vol. 10, pp. 215-227.

21. J. S. Koehler, "The Nature of Work-Hardening," Physics Review (1952), Vol. 86, pp. 52-59.

22. J. D. Eshelby, "Dislocations as a Cause of Mechanical Damping in Metals," Proceedings of the Royal Society of London (1949), Vol. 197A, pp. 396-416.

23. W. G. Johnston, "Yield Points and Delay Times in Single Crystals," Journal of Applied Physics (1962), Vol. 33, pp. 2716-2730.

REFERENCES--Continued

24. A. H. Cottrell, "Discontinuous Yielding," The Relation between the Structure and Mechanical Properties of Metals (1963), Her Majesty's Stationary Office, London, pp. 456-473.

25. N. J. Petch, "The Upper Yield Stress of Polycrystalline Iron," Acta Metallurgica (1964), Vol. 12, pp. 59-65.

26. H. W. Schadler, "Mobility of Edge Dislocations on {110} Planes in Tungsten Single Crystals," Acta Metallurgica (1964), Vol. 12, pp. 861-870.

27. J. C. Suits and J. R. Low, Jr., "Dislocation Etch Pits in Silicon-Iron," Acta Metallurgica (1957), Vol. 5, pp. 285-289.

28. C. G. Dunn and G. C. Nonken, "Production of Oriented Single-Crystal Silicon-Iron Sheet," Metal Progress (1953), December, pp. 71-75.

29. Letter from J. R. Low, Jr. to D. S. Wood (August 24, 1965).

30. T. L. Russell, D. S. Wood and D. S. Clark, First Interim Technical Report under Office of Ordnance Research, Contract No. DA-04-495-ORD-171, California Institute of Technology, 1955.

31. W. M. Murray and D. K. Stein, Strain Gage Techniques (1958), Massachusetts Institute of Technology, Cambridge, Mass., p. 249.

32. C. S. Barrett, Structure of Metals (1952), McGraw-Hill, Inc., New York, p. 193.

33. Ibid., p. 370.

34. D. Hull, "Orientation and Temperature Dependence of Plastic Deformation Processes in 3.25% Silicon-Iron," Proceedings of the Royal Society of London (1963), Vol. 274A, pp. 5-20.

35. Barret, op. cit., p. 337.

36. Ibid., p. 379.

37. P. J. Worthington and E. Smith, "The Formation of Slip Bands in Polycrystalline 3% Silicon-Iron in the Pre-Yield Microstrain Region," Acta Metallurgica (1964), Vol. 12, pp. 1277-1281.

REFERENCES--Continued

38. D. McLean, Mechanical Properites of Metals (1962), John Wiley and Son, New York, p. 6.

39. W. R. Hibbard, Jr. and C. G. Dunn, "A Study of ⟨112⟩ Edge Dislocations in Bent Silicon-Iron Single Crystals," Acta Metallurgica (1956), Vol. 4, pp. 306-315.

40. E. W. Hart, "A Uniaxial Strain Model for a Luder's Band," Acta Metallurgica (1955), Vol. 3, pp. 146-149.

41. R. W. Guard,"Rate sensitivity and dislocation velocity in silicon-iron," Acta Metallurgica (1961), Vol. 9, pp. 163-165.

42. F. W. Noble and D. Hull, "Stress dependence of dislocation velocity from stress relaxation experiments," Acta Metallurgica (1964), Vol. 12, pp. 1089-1092.